A new instrument for stable isotope measurements of ^{13}C and ^{18}O in CO$_2$ - Instrument performance and ecological application of the Delta Ray IRIS analyzer

Jelka Braden-Behrens[1], Yuan Yan[1], and Alexander Knohl[1,2]

[1]University of Goettingen, Bioclimatology, Faculty of Forest Sciences and Forest Ecology, Germany
[2]University of Goettingen, Centre of Biodiversity and Sustainable Land Use (CBL), Germany

Correspondence to: Jelka Braden-Behrens (jbraden1@gwdg.de)

Abstract.

We used the recently developed Delta Ray Isotope Ratio Infrared Spectrometer (IRIS) to continuously measure the CO$_2$ concentration c and its isotopic composition δ^{13}C and δ^{18}O in a managed beech forest in Central Germany. Our objectives are (a) to characterize the Delta Ray IRIS and its performance under field conditions and (b) to quantify the seasonal variability

5 of c, δ^{13}C, δ^{18}O and the isotopic composition of CO$_2$ exchange (R_{eco}^{13}C and R_{eco}^{18}O) derived from nighttime Keeling-Plot intercepts. The minimal Allan deviation (as a measure of precision) was below 0.01 ppm for the CO$_2$ concentration and below 0.03‰ for both δ values. For repeated measurements of a target gas, the long-term standard deviation from the mean value was 0.2 ppm for c and below 0.3‰ for both δ values. The accuracy based on our calibration setup was approximately 0.45 ppm for c, 0.1‰ for δ^{13}C and 0.6‰ for δ^{18}O. We used measurements of nine different inlet heights in the beech forest,

10 to evaluate the isotopic compositions of respiration R_{eco}^{13}C and R_{eco}^{18}O in a three months measurement campaign in autumn 2015. During this period, an early snow and frost event occurred, coinciding with a change in the observed characteristics of both R_{eco}^{13}C and R_{eco}^{18}O . Before the first snow, R_{eco}^{13}C correlated significantly (Pearson correlation coefficient $r_{pear}\approx0.55$ and corresponding critical value $r_{crit}\approx0.38$ for $\alpha=0.005$) with time-lagged net radiation R_n, a driver of photosynthesis and photosynthetic discrimination against ^{13}C . This correlation became insignificant after the first snow. For ^{18}O, we measured a

15 decrease of 30‰ within 10 days in R_{eco}^{18}O after the snow event potentially reflecting the influence of ^{18}O depleted snow on soil moisture. This decrease was ten times larger than the corresponding decrease in δ^{18}O in ambient CO$_2$ (below 3‰) and took three times longer to recover (three weeks vs. one week). In summary, we conclude that 1) the new Delta Ray IRIS with its internal calibration procedure provides an opportunity to precisely and accurately measure c, δ^{13}C and δ^{18}O at field sites and 2) even short snow or frost events could have strong effects on the isotopic composition of CO$_2$ exchange at ecosystem

20 scale.

1 Introduction

The stable isotopic compositions of CO$_2$ and water vapor have been intensely used to study ecosystem gas exchange (Yakir et al., 2000). In particular, measurements of the δ^{13}C and δ^{18}O isotopic composition of CO$_2$ have provided important insights

into the carbon cycle over a large variety of spatial and temporal scales (Flanagan and Ehleringer, 1998; Affek and Yakir, 2014). There are many examples for the utility of the stable isotopic composition of CO_2 to study biosphere-atmosphere exchange processes on ecosystem scale, such as the partitioning of net ecosystem CO_2 exchange into respiration and photosynthesis. Different partitioning methods include the combination of gradient approaches with stable isotope measurements (Yakir and

5 Wang, 1996), direct isotopologue gradient approaches (Zhang et al., 2006), the combination of eddy covariance measurements with isotope flask measurements (Bowling et al., 2001; Ogée et al., 2003; Knohl and Buchmann, 2005), and direct eddy covariance measurements for isotopologues (Wehr et al., 2016; Oikawa et al., 2017). Another example for the use of stable isotopes in CO_2 to investigate ecosystem gas exchange, is the analysis of the temporal variability of the isotopic composition of a particular flux component. The temporal variability of respiration for example has been studied on timescales ranging

10 from sub-diurnal (Barbour et al., 2011) to seasonal (Ekblad and Högberg, 2001; Bowling et al., 2002; Knohl et al., 2005). The mentioned studies on seasonal scale also used the temporal variability of the isotopic composition of respiration to assess the time lag between assimilation and respiration.

A long established and broadly used technique to measure stable isotopic compositions is Isotope Ratio Mass Spectrometry (IRMS), with typical precisions of approximately 0.02 to 0.1‰ for ^{13}C and 0.05 to 0.2‰ for ^{18}O in CO_2 (Griffis, 2013). In

15 general, the concept of mass spectrometers, developed by Thomson (1908), is based on the fact that moving ions with different mass-to-charge ratio can be separated by (orthogonal) magnetic fields. IRMS has been widely used for isotope studies in environmental sciences, but shows limited applicability for *in situ* meteorological measurements - reasons for this include high sample preparation effort and costs (Griffis, 2013). Progress in optical based techniques for isotopic measurements over the last decade enhanced the potential of measurements of isotopic compositions (Werner et al., 2012). These developments have

20 a particular impact on micrometeorological studies, as they increased the accessibility of field-deployable optical instruments and thus enabled a number of micrometeorological applications of stable isotope techniques, as reviewed by Griffis (2013).

Optical instruments to study the isotopic composition of trace gases use the absorption of infrared photons by exciting a molecules rotational and vibrational energy states. These rotational and vibrational transitions are characteristically different for molecules, composed of different stable isotopes (isotopologues) (Esler et al., 2000; Kerstel and Gianfrani, 2008). The

25 characteristic absorption lines for the different isotopologues of a molecule are related to the isotopologues concentrations via Beer's law and thus the isotopic composition of a certain molecule (Werle, 2004). The available optical instruments that are capable of measuring isotopic compositions at trace gas concentrations show different implementations of this principle: One major classification of optically based instruments can be done with respect to the light source that is used, between 1. broadband light source based instruments and 2. laser based instruments (Griffis, 2013). Fourier Transform Infrared (FTIR)

30 Spectrometers, as e.g. the Spectronus analyzer *Ecotech Pty Ltd., Knoxield, Australia* (Griffith et al., 2012), belong to the first of these categories. In these kind of instruments, the complete infrared spectrum of a black body light source is used (Griffith et al., 2012). The emitted infrared light is modulated by a Michelson interferometer and the resulting interferogram is recorded and converted into the absorption spectrum mathematically by applying a Fourier transformation (Griffith et al., 2012, citing Davis et al., 2001 and Griffiths et al., 2007). In laser based absorption spectrometers on the other hand, a laser beam with

35 tunable wavelength is sent through a (multi-path or resonant) absorption cell, usually operating at low pressure, and the light

intensity of the emerging laser beam is measured by a suitable detector (Werle, 2004). Laser based instruments have been described in detail by Kerstel and Gianfrani (2008), who provide a further classification for laser-based measurements at trace gas concentrations. In slightly different words, these categories can be named (a) direct laser absorption spectrometers in mid infrared where strong absorption features are available and (b) laser absorption spectrometers in near infrared that compensate

5 the weaker absorption in the near infrared by a strongly enhanced effective optical path length.

Different laser spectrometers of the above mentioned category of instruments 2.(a) use different lasers to achieve a laser beam in the desired mid infrared region (Kerstel and Gianfrani, 2008). Examples for such different laser types in laser absorption spectrometers are the quantum cascade lasers in QCLAS-instruments, *Aerodyne Research. Inc, Boston, USA* (Sturm et al., 2012; Wehr et al., 2016) and CCIA-48 *Los Gatos Research. Inc, San Jose, USA* (Oikawa et al., 2017), or the lead-salt tunable

10 diode lasers, in the TGA100A/200 instruments, *Campbell Scientific Inc., Logan, USA* (Bowling et al., 2003c). For instruments of class 2.(b) there are two major technical implementations that both increase the optical path length by using high finesse optical cavities yielding a better signal-to-noise ratio (Kerstel and Gianfrani, 2008). Both of these implementations are related to the decay of light intensity after the laser is switched of (Griffis, 2013): Cavity Ringdown Spectroscopy (CRDS), e.g. the G1101-i and G1101-i+ *Picarro Inc.,Santa Clara, USA* see e.g. (Vogel et al., 2013), and Off-Axis Integrated Cavity Output

15 Spectroscopy (OA-ICOS), e.g. the CCIA DLT-100 *Los Gatos Research Inc., San Jose, USA* see e.g. (Guillon et al., 2012). Minimal Allan deviations σ_A and the corresponding averaging times $\tau_{\min}$ for different optical based instruments of all three different categories are shown in Table 2, but see also Table 2 in the review of Griffis (2013) for more detailed information, including instrument stability and an overview of applications, for most of these instruments.

Here we present a new laser based instrument, the Isotope Ratio Infrared Spectrometer (IRIS) Delta Ray, *Thermo Scientific*

20 *Inc., Waltham, USA*, that belongs to category 2.(a): A direct laser absorption spectrometers in mid infrared. This spectrometer uses a nonlinear crystal in combination with two tunable near infrared diode lasers to produce a laser beam in the mid infrared, at approximately $4.3\,\mu$m (Thermo Fisher Scientific, 2014). The instrument has a flow rate of 0.08 slpm, a cell pressure of approximately 100 mbar, an optical path length of approximately 5 m and an internal calibration procedure that automatically includes two point calibrations for concentration c and both δ values as well as corrections for the concentration dependency of

25 the measured δ-values (Thermo Fisher Scientific, 2014). The objectives of our study are (a) to characterize the Delta Ray IRIS and its performance under field conditions as well as (b) to quantify the seasonal variability of δ^{13}C, δ^{18}O and the isotopic composition of CO_2 exchange for both δ^{13}C and δ^{18}O derived from Keeling-Plot intercepts. We measured the internal cell turnover to capture the maximum sampling frequency of physically different samples. Additionally, we measured the Allan deviation to assess the instruments precision and performed accuracy measurements using a gas tank with known isotopic

30 composition. We assessed long-term stability of the instrument by performing repeated tank measurements. For the ecological application, we installed the instrument in a beech forest in Central Germany, characterized the seasonal variability of the isotopic composition of CO_2 exchange (R_{eco}^{13}C and R_{eco}^{18}O), and analyzed the correlation between the seasonal variability of R_{eco}^{13}C and different meteorological variables.

2 Material and methods

2.1 Field site

This study was conducted at a meteorological tower in a managed beech forest (*Fagus sylvatica L.*) in Thuringia (Central Germany) at 51°19'41,58" N; 10°22'04,08" E at 450 meters above sea level. The forest in the dominant wind direction of the tower has a canopy height of approximately 35 m with a top-weighted canopy and a very homogeneous stand structure containing trees of three age classes (30–40, 80 and 160 years). The field site is described in detail by Anthoni et al. (2004) and soil characteristics of this site were analyzed by Mund (2004).

2.2 Campaign design

We measured the CO_2 concentration c and its isotopic composition $\delta^{13}C$ and $\delta^{18}O$ in ambient air from 21. August 2015 to 16. November 2015. We measured these quantities with the field deployable Isotope Ratio Infrared Spectrometer (IRIS) Delta Ray (*Thermo Scientific, Waltham, USA*) at nine inlet heights ranging from 0.1 to 45 m in an automatic measurement setup. Each inlet was measured for 80 s, (consisting of four physically different air samples, averaged over 20 s separately) after the tubing was purged for 60 s. A full measurement cycle took 30 minutes and consisted of measurements of all nine inlet heights and a target standard (CO_2 in synthetic air with known concentration and isotopic composition, details for the gas tank are given in Sect. 2.4), supplemented by an internal calibration measurement. In less detail the experimental setup is also described in (Braden-Behrens et al., 2017).

We used the nighttime measurements of c, $\delta^{13}C$ and $\delta^{18}O$ of the different inlet heights in a Keeling-Plot approach (Keeling, 1958) to calculate the nighttime Keeling-Plot intercept that can be used to estimate the isotopic composition of ecosystem respiration δR_{eco} for both measured δ values: ^{13}C and ^{18}O. Additionally, we used the half hourly measurements of the target standard to track the temporal stability of the Delta Ray analyzer and performed additional (manual) measurements to analyze the analyzer's characteristics.

2.3 Application of the Keeling-Plot approach

The Keeling-Plot approach (Keeling, 1958) is based on a simple two-component mixing model that describes how air from a source with effectively constant isotopic composition δ_s mixes with a background (with constant c_{bg} and δ_{bg}). For this simple two-component mixing model, one can derive a linear relationship between the measured isotopic composition δ_{meas} and the reciprocal concentration $1/c_{meas}$ by applying conservation of mass for the total concentration as well as for each isotopologue separately, for derivation see e.g. (Pataki et al., 2003).

$$\delta_{meas} = \underbrace{(\delta_{bg} - \delta_s)\, c_{bg}}_{m_{KP}} \; \frac{1}{c_{meas}} + \underbrace{\delta_s}_{\delta_{KP}} \tag{1}$$

This linear relationship with slope m_{KP} and intercept δ_{KP} can be derived for each isotopic species independently, so in our case for both $\delta^{13}C$ or $\delta^{18}O$. The applicability of the Keeling-Plot approach to a certain experimental setup essentially depends

on the question if c_{bg}, δ_{bg} and δ_s are effectively constant over the spatial and temporal distribution of all measurements that are taken into account for the linear regression. In this study we apply a Keeling-Plot approach to a forest ecosystem, aiming at measuring the isotopic composition of ecosystem integrated CO_2 exchange. The source of CO_2 is thus composed of different individual source components i (e.g. stem, leaf and soil respiration), each accounting for the individual components with their

5 isotopic compositions $\delta_{s,i}$. The corresponding isotopic composition of the integrated source δ_s can be expressed by defining α_i, as the relative contributions of the individual source components to the integrated source.

$$\delta_s = \sum_i \delta_{s,i} \, \alpha_i \qquad \text{with:} \qquad \sum_i \alpha_i = 1 \qquad\qquad (2)$$

If the relative distributions among the different source components α_i produce significant changes in δ_s over the spatial and temporal distribution of measurements, the basic two component assumption of stable δ_s is violated. During daytime the appli-

10 cation of a Keeling-Plot approach on ecosystem scale in a forest is in general problematic, as photosynthesis and respiration are two separately controlled and spatially separated processes - so we generally can not assume spatiotemporally constant α_i. But for nighttime, when there is only respiration, the nighttime Keeling-Plot intercept δ_{KP} can be interpreted as the isotopic composition of respiration $\delta^{13}C\,R_{\mathrm{eco}}$ or $\delta^{18}O\,R_{\mathrm{eco}}$. Measures to assure and test the applicability of this two component approach and to improve the quality of the calculated Keeling-Plot intercepts are discussed and evaluated in appendix A. In brief, they

15 include the minimization of the sampling time for each Keeling-Plot, an inclusion of all inlet heights into each Keeling-Plot analysis to increase the CO_2 concentration range, data filtering and weighted averaging of Keeling-Plots on smaller timescales.

2.4 Material and technical specifications

Technical specifications of the setup including plumbing and the automatic switching unit are shown schematically in Fig. 1. The automatic switching unit consisted of ten electromagnetic 3/2-way valves (Fig. 1) and was operated by a PC using

20 a software for measuring technology (ProfiLabExpert 4.0, Abacom, Germany). The operating software controlled the valve positions using two USB relay boards (Abacom, Germany). When switching the valves to a new position, the operating software additionally sent a 1 s long rectangular trigger pulse with 5 V DC to one of the Delta Ray analyzer's two different analogue input channels. One of these channels was used when a target gas measurement had to be started while a trigger pulse at the other input channel initialized the height measurements. After the Delta Ray analyzer received one of the trigger pulses, the

25 tubes and the measurement cell were purged for 60 s before the analyzer took measurements for 80 s. This purging time was used to ensure that the analyzer took physically separated measurements for the different inlets.

We used poly ethylene (PE) tubes with 6 mm outer diameter and 4 mm inner diameter (Landefeld GmbH, Kassel, Germany) for the plumbing in the switching unit as well as for the nine height inlets. These inlets were additionally equipped with biweekly changed 1.2 μm PTFE membrane filters (Rettberg GmbH, Göttingen, Germany). The tubes for the height inlets

30 were all equally long (50 m) - except the highest height that had to be extended to 52 m for practical reasons. The equal (or similar) length of the inlet tubes lead to similar flow rates in the tubing system and similar inlet pressures for the analyzer regardless of the valve position. Thus, we decreased pressure jumps after switching from one height position to another. We continuously purged all nine height inlet tubes using an additional purging pump to avoid condensation in the tubes (Fig.

1). Thus, the flow rate in the height inlet tubes was approximately 1.5 slpm for all heights all the time and the major part of the gas flow was directed into the purging pump. In case of the target standard, the tubing was only purged when the target standard was measured. In this case an overblow opened to enable gas release at approximately 1 slpm (Fig. 1). For the target measurements as well as for the height measurements the analyzer took a sub-sample of the corresponding inlet line with a

5 flow rate of approximately 0.08 slpm. Because condensation could occur especially in the tubes with this small flow rate and at the valves, we heated the valve box and all tubes that were not continuously purged with higher flow rates. For heating we used self-regulating heating wires (Horst GmbH, Lorsch, Germany) that produce a constant temperature of 65°C.

For the half-hourly performed target standard measurements, the manual measurements of different additional gas tanks and for calibration, we used gas tanks in 50 l steel containers at 150 to 200 bar pressure containing synthetic air, synthetic air with

10 different CO_2 concentrations and pressurized air (Westfalen AG, Gleichen, Germany). For calibration, we additionally used two 1 l gas tanks at 10 bar pressure with pure CO_2 at different (known) δ values that were shipped with the Delta Ray analyzer (Air Liquide, Düsseldorf, Germany). All CO_2 containing gas tanks that were used for calibration as well as the target gas tank were measured high precisely for their CO_2 concentration and isotopic composition in ^{13}C and ^{18}O at the Max Planck Institute for Biogeochemistry in Jena. Due to the limited availability of gas tanks with atmospheric (and high precisely measured)

15 δ values, the gas tank that was used for accuracy measurements ('PA-tank', c.f. Table 3) was a secondary standard which was measured in the field using an independently calibrated quantum-cascade laser based absorption spectrometer (QCLAS, *Aerodyne Research Inc.*, Boston, USA). All known δ-values and concentrations for the gas tanks used in this application can be found in Table 3 with their corresponding uncertainties.

2.5 Instrument characterization measurements

20 We quantified the Delta Ray analyzer's long term stability under field conditions as well as its precision, accuracy and cell turnover by the following approaches: The analyzers long term stability under field conditions could be quantified by directly analyzing the half hourly performed target measurements described in Sect. 2.4. For further instrument characterization, we carried out additional measurements that involved changes in the plumbing. For all measurements that required connecting different gas tanks to the analyzer, the plumbing was equivalent to the plumbing of the target gas (Fig.1). We measured

25 the Allan deviation by connecting pressurized air at atmospheric delta values to the analyzer and took measurements at the analyzer's maximum data acquisition rate of 1 Hz for two hours. Due to limited supply of gas cylinders at ambient delta values at the field site, this experiment was done in the laboratory before the Delta Ray analyzer was transported to the field site. To quantify the Delta Ray analyzer's accuracy, we replaced the target standard with a gas tank with ambient δ values 'PA-tank' (c.f. Table 3) and measured this tank for approximately 10 minutes with a measurement frequency of 1 Hz. The cell turnover was

30 measured by using the automatic switching unit to switch from ambient air (height 1) to the target standard. We superimposed the measurements of four switching events to observe the adjacent turnover processes.

2.6 Meteorological measurements

Supplementary to the measurements with the Delta Ray analyzer, the meteorological tower at the field site is equipped with an Eddy Covariance system to measure CO_2 and H_2O_v fluxes as well as latent and sensible heat fluxes. Additional standard meteorological measurements include continuous measurements of short wave and long wave radiation, wind speed and direction, precipitation, air and soil temperature and air and soil humidity (Anthoni et al., 2004).

2.7 Calibration

2.7.1 Instrument internal calibration

The Delta Ray analyzer is equipped with three different instrument-internal calibration routines (Thermo Fisher Scientific, 2014). We performed these routines at the field site (in situ) each time the analyzer had to be restarted e.g. after power supply failures, instrument issues or when we manually turned off the analyzer for other reasons. All three instrument internal calibration procedures were usually done one day after restarting the analyzer, thus the instrument was in thermal equilibrium during calibration. We used the three analyzer's internal calibration routines (Thermo Fisher Scientific, 2014) in the following way:

- „Linearity calibration"
  This calibration routine evaluates the concentration dependency of δ-value measurements. In our setup the pure CO_2 with near to ambient δ-values (tank 'ambient CO_2', c.f. Table 3) was automatically mixed with synthetic air to produce gas with constant δ values at different concentrations ranging from approximately 150 to 3500 ppm CO_2 (Braden-Behrens et al., 2017).

- „Delta scale calibration"
  This calibration routine is based on a two-point-calibration of δ values using two tanks of pure CO_2 with different δ values, that are diluted with synthetic air (using two pure CO_2 tanks 'ambient CO_2' and 'bio CO_2', c.f. Table 3).

- „Concentration calibration "
  This calibration routine performs a two-point-calibration for CO_2 concentration using two gas tanks with different CO_2 concentrations. We performed this measurement simultaneously to the other two calibration routines in the field, but we could improve the accuracy by performing a post-processing concentration calibration, described in Sect. 2.7.2.

Additionally to these three instrument internal calibration procedures, we measured the pure CO_2 standard ('ambient CO_2', c.f. Table 3) diluted with synthetic air at a freely selectable concentration every 30 minutes as a part of our repetitive measurement cycle. This is implemented in the so called „referencing" in the Delta Ray analyzers software QTEGRA. We chose the reference concentration to be the same as in the highest inlet in the adjacent cycle, because most of the measurement inlets had delta values close to the values measured at the highest inlet and the temporal variability of the measured concentrations generally decreased with height. Thus, we achieved to perform the referencing as close as possible to as many height measurements as possible by these settings.

2.7.2 Post processing for concentration calibration

Measurements with five different gas tanks with known CO_2-concentrations ranging from 350 to 450 ppm in the field resulted in considerably high deviations of the (instrument-internal in-situ calibrated) concentrations from known concentrations (high precisely measured at the Max Planck Institute for Biogeochemistry in Jena). In average this deviation was 0.8 ± 0.2 ppm.

5 A possible reason for this resulting deviation is the range of the gas tanks we used for the instrument-internal concentration calibration, that was approximately 300 to 430 ppm. As the half-hourly performed measurement of the target standard ('SACO2-tank' c.f. Table 3) showed a very stable behavior (see Sect. 3.1.3), and in especially no jumps occurred when the analyzer was re-calibrated in the field, we used two of these external measurements of known standards with a wider concentration range ('LS-tank' with approximately 350 and 'HS-tank' with approximately 450 ppm CO_2, c.f. Table 3) to post-calibrate

10 the measured concentrations using a simple two point calibration. With this calibration procedure, we could reduce the mean deviation of the three remaining measured tanks from the corresponding high precise lab measurements from 0.8 ± 0.2 ppm down to in average 0.3 ± 0.1 ppm.

2.8 Multilayer modeling

We used the multilayer model CANVEG to calculate the isotopic composition of assimilated material $\delta^{13}C_{Ass}$. CANVEG

15 is a biophysical one-dimensional multilayer canopy model, see e.g. (Baldocchi, 1997; Baldocchi and Wilson, 2001). This multilayer model uses hourly meteorological inputs (among others temperature, radiation, vapor pressure deficit, wind velocity and CO_2 concentration) as main drivers, as well as site specific parameters (leaf area index, leaf clumping status, canopy height et. al.). Based on these input variables, CANVEG iteratively computes the biosphere-atmosphere exchange of water, carbon dioxide and energy as well as the microclimate within and above the canopy at hourly time steps. The carbon, water

20 and energy modules have been validated for various environmental conditions and forest types, see e.g. (Baldocchi et al., 1997, 1999, 2002). In particular, the model has also been applied to an unmanaged beech dominated forest field site in approximately 30 km air-line distance to the measurement site of this study (Knohl and Baldocchi, 2008). The isotope enabled version of this model additionally calculates the ^{13}C composition of CO_2 $\delta^{13}C_{ij}$ for each canopy layer i and each hourly timestep j and the corresponding ^{13}C composition of assimilated material $\delta^{13}C_{Ass,ij}$ (Baldocchi and Bowling, 2003). In our application, we set

25 up the model to use 40 equally thick layers i and we used our meteorological measurements at the field site, described in Sect. 2.6, as input variables. We validated the model with Eddy Covariance measurements (Table 4) and used the model to calculate the isotopic composition of assimilated material $\delta^{13}C_{Ass,ij}$ for each of the 40 canopy layer i and for each hourly time step j. The ^{13}C composition of assimilated material $\delta^{13}C_{Ass}$ on daily timescale was calculated as an assimilation weighted sum over all layers and time steps, with the modeled assimilation rate A_{ij} as a weighting factor:

$$\delta^{13}C_{Ass} = \frac{\sum_{i=1}^{40} \sum_{j=1}^{24} A_{ij} \cdot \delta^{13}C_{Ass,ij}}{\sum_{i=1}^{40} \sum_{j=1}^{24} A_{ij}} \tag{3}$$

We included only hours j and layers i during photosynthesis (with positive assimilation rates). We analyzed the correlation of modeled $\delta^{13}C_{Ass}$ to net radiation R_n, a driver of photosynthesis and photosynthetic discrimination, during our measurement

period in autumn 2015. We further compared the resulting relationship between R_n and $\delta^{13}C_{\text{Ass}}$ to the observed relationship between R_n and the ^{13}C composition of respiration R^{13}_{eco}C, derived from the measured Keeling-Plots.

3 Results and discussion

3.1 Instrument characteristics

5 #### 3.1.1 Precision

We use the Allan deviation σ_A at different averaging times τ (Table 5) to characterize the Delta Ray IRIS analyzer's precision. Starting at an averaging time of 1 s, that corresponds to the IRIS analyzers maximum data acquisition frequency, the Allan deviation σ_A decreased with $\tau^{-1/2}$ (Fig. 2). This matches the expected behavior of a system that is dominated by white frequency noise. The measured Allan deviation σ_A followed this slope up to averaging times for approximately 300 s for
10 δ value measurements and approximately 200 s for concentration measurements. At these timescales the analyzer showed its maximum precision of 0.02 ‰ VPDB for δ^{13}C, 0.03 ‰ VPDB-CO2 for δ^{18}O and 0.007 ppm for CO_2 concentration. For averaging times above 200-300 s other error sources (such as instrument drift) became significant. For δ^{13}C, the precision of an earlier version of the instrument has also been measured by Geldern et al. (2014), reporting a minimum of σ_A at around 0.04 ‰ for an averaging time of $\tau \approx 550$ s. At this averaging time, we measured an Allan Deviation below 0.03 ‰ (c.f. Table 5).
15 Two other averaging times are particularly interesting for our application: Firstly, we chose an averaging period of 20 s that yields Allan variances below 0.1 ‰ for both δ values and 0.02 ppm for CO_2 concentration to solve the trade-off between higher precision and a larger number of measurements. Secondly we set the IRIS analyzer's internal referencing procedure (described in Sect. 2.7) to 1800 s which corresponds to an Allan variance of 0.03 ‰ for both δ values and 0.01 ppm for CO_2 concentration.

20 #### 3.1.2 Accuracy

The instrument's accuracy was defined as the mean deviation of N=300 field measurements of a tank with pressurized air ('PA-tank', c.f. Table 3) from its known (independently measured) values. The frequency distribution for these measurements is shown in Fig. 3). The so defined accuracy was below 0.1 ‰ VPDB for δ^{13}C, 0.6 ‰ for δ^{18}O and 0.45 ppm for CO_2 concentration. To evaluate this measured accuracy, we compare it to the setup-dependent expected uncertainty which we define as
25 the sum of the uncertainties of the calibration tanks ('bio CO_2' and 'ambient CO_2' for δ values 'LS-tank' and 'HS-tank' for concentration) and the uncertainty of the pressurized air tank used for the accuracy test 'PA-tank' (Table 3). The so defined expected uncertainty sums up to approximately 0.2 ‰ VPDB for δ^{13}C, 0.7 ‰ for δ^{18}O and 0.3 ppm for CO_2 concentration. Thus the measured uncertainty was below the expected uncertainty in the case of δ^{13}C and δ^{18}O, but it was higher than the expected uncertainty for concentration measurements. In the case of δ^{18}O this is remarkable because the corresponding calibration tanks
30 spanned only a range of -17.5 ‰ to -27.2 ‰ (c.f. Table 3), whereas the pressurized air used here 'PA-tank' had δ^{18}O value of -5.3 ‰. In the case of CO_2 concentration the observed deviation from the expected accuracy might arise from the simple two

point calibration we had to perform in a post processing step due to practical limitations (see Sect. 2.7.2). Considering these limitations of our calibration setup the measured accuracy seems reasonable to reflect the accuracy of our long-term set up under field conditions.

3.1.3 Long-term stability

5   We analyzed the long-term stability of the Delta Ray analyzer under field conditions by evaluating half-hourly measurements of the same gas tank (SA-CO2-5) during the whole measurement period. We use the standard deviations and mean drift extrapolated to a period of 100 days to quantify the long term stability of our set up in the field including our calibration strategy. The standard deviations of these long-term measurements were below 0.2 ppm for CO_2 concentration and below 0.3 ‰ for both δ values (frequency distributions and time series of the long term measurements are shown with color-coded

10   metadata in Fig. 4. The instrument drift, a measure for the instrument's long-term stability, was below 0.04 ‰/100 d for δ^{13}C, 0.3 ‰/100 d for δ^{18}O and 0.3 ppm/100 d for CO_2-concentration. Thus, the long term stability measured here is comparable to the measured accuracy of our set up, described in the preceding paragraph.

3.1.4 Turnover time

  We measured the turnover behavior of our system (tubing and measurement cell of the Delta Ray IRIS) by using the valve

15   system shown in Fig. 1 to switch from ambient air with δ^{13}C≈-9 ‰ and δ^{18}O≈1 ‰ to tank air with δ^{13}C≈-38 ‰ and δ^{18}O≈-36 ‰. The time series of the measured δ-values after the change of the valve position consisted of three different phases that can be related to different physical processes, shown in Fig. 5: Within a first phase of turnover, the measured δ-values remained constant for $\tau_1 \approx 14$ s. This is the setup specific-time it took for the gas to flush the tubes and valves before entering the cell. As a second phase of turnover, we measured a quadratic decay of the measured δ-values, which we can relate

20   to mixing of gas within the tubes (before it enters the cell). This phase dominated the turnover of our system for $\tau_2 \approx 4.5$ s. The third phase of turnover is the exponential decay with a characteristic decay time (defined here using the 10 %-threshold) $\tau_{10\%} \approx 10$ s for δ^{13}C and $\tau_{10\%} \approx 11$ s for δ^{18}O. This exponential behavior can be derived for an idealized situation that includes perfect mixing in a volume V_{mix} yielding:

$$\tau_{10\%} = \frac{log(10) \cdot p_{\mathrm{cell}} \cdot V_{\mathrm{mix}}}{\Phi}$$

25   With flow rate Φ, cell pressure p_{cell} and effective mixing volume V_{mix}. Using the volume of the measurement cell as an upper threshold for the effective mixing volume within the cell: $\max(V_{\mathrm{mix}}) = V_{\mathrm{cell}} = 80$ ml, we can calculate an upper threshold for $\tau_{10\%}$. With the instruments flow rate of $\Phi = 0.08$ slpm and the cell pressure of $p_{\mathrm{cell}} \approx 100$ mbar we get $\tau_{10\%,\mathrm{max}} \approx 13.6$ s. Thus the measured value of $\tau_{10\%,\mathrm{max}}$ is slightly below this value, indicating $V_{\mathrm{mix}} < V_{\mathrm{cell}}$. We define the total turnover time τ_{tot} as the time-span it took until the step change between the two inlets reached 0.1 % of the corresponding difference in δ

30   values, with $\tau_3 = \tau_{0.1\%} = 3 \cdot \tau_{10\%}$. The three different phases of turnover (tube transport, tube mixing dominated change and cell mixing dominated change) summed up to a net turnover time $\tau_{\mathrm{tot}} = \tau_1 + \tau_2 + \tau_3 < 60$ s. Thus, the cell flushing time of our application (60 s) is appropriate to produce independent measurements of two different inlets.

3.1.5 Utilization rate, power consumption and maintenance effort

We define the utilization rate as the number of successfully recorded measurement cycles divided by the number of measurement cycles that were theoretically possible during the field campaign (approximately 4200). This can be calculated separately for a) profile measurements and b) target gas measurements, because some data gaps were specific for target measurements.

5 The utilization rate for was approximately 80 % for measurements of the height profile and approximately 70 % for target gas measurements. Two major reasons for data gaps reduced the utilization rate for both, profile and target measurement by 5 % (a laser alignment problem that could be resolved after 4 days) and 6 % (three data acquisition problems, the longest lasting three days). Additionally, four external power supply problems at the field site lead to a further reduction of the utilization rate by 3.3 %. These data gaps, as well as smaller datagaps, that reduced the utilization rate are listed in Table 7. In the case of target

10 measurements, the main reason for data gaps (accounting for a reduction of utilization rate of more than 9 %) were plumbing issues that lead to a contamination of the target gas by ambient air. Thus a more stable target plumbing would be a promising approach to increase the utilization rate, as well as a more stable power supply and more frequent field trips.

Maintenance effort and power consumption of the whole setup were moderate: The analyzer's power consumption of approximately 220 W was slightly smaller than the power consumption of the basic infrastructure of the setup that included the

15 heated valve box and its controlling unit (see Table 6). To maintain and to control the setup we went to the field site weekly or biweekly and used remote access to the instrument via a satellite connection.

3.2 Ecological Application

3.2.1 Time series of measured quantities

The measured CO_2 concentrations in 45 m height in a managed beech forest in Central Germany ranged from 385 to 450 ppm

20 with corresponding δ values between -11 to -7‰ for ^{13}C and between -6 and 2‰ for ^{18}O over a three-month period in autumn 2015 (Fig. 6). As the lower heights commonly contain larger amounts of respired (typically lighter) CO_2, the lower inlets show larger CO_2 concentrations c with smaller δ values. We calculated a three-month time series of nighttime Keeling-Plot intercepts $\delta^{13}C_{KP}$ and $\delta^{18}O_{KP}$ (shown with temperature and precipitation data in Fig. 7), that can be interpreted as the respective isotopic composition of ecosystem respiration $R^{13}_{eco}C$ and $R^{18}_{eco}O$. A particular feature of the measurement period

25 is an early snow and frost event with negative temperatures during four nights between 11. and 15. October 2015 (Fig. 7). The corresponding snow event on 13. October could be identified on a canopy picture, taken at midday on 13. October 2015. The time of the snow and frost event coincided with changes in the characteristics of δ^{18}O, $R^{18}_{eco}O$ and $R^{13}_{eco}C$: For δ^{18}O and $R^{18}_{eco}O$ a strong decrease was obtained after the snow event. This decrease was the largest signal in the respective time series. For $R^{13}_{eco}C$, the analysis of its potential meteorological drivers yielded different results for the time periods before and after the

30 first snow. Additionally, according to Eddy Covariance measurements the forest was a net CO_2 sink with negative diurnal net ecosystem exchange (NEE) before the 12. October (with only one exception), whereas it was a net CO_2 source with positive diurnal NEE after the snow event on 13. October (also with only one exception).

3.2.2 Potential drivers for $R_{\mathrm{eco}}^{13}\mathrm{C}$

Previous studies linked the temporal variability of the ^{13}C composition of ecosystem respiration $R_{\mathrm{eco}}^{13}\mathrm{C}$ partially to changes in the meteorological conditions during photosynthesis, namely relative humidity RH, Vapor pressure deficit VPD, photosynthetically active radiation (PAR) and the ratio VPD/PAR (Ekblad and Högberg, 2001; Bowling et al., 2002; Knohl et al.,

5 2005). These links occurred with time lags, that correspond to the time lag between assimilation and respiration, which is approximately four to five days for mature trees (Kuzyakov and Gavrichkova, 2010). The observed time lagged links between meteorological variables and $R_{\mathrm{eco}}^{13}\mathrm{C}$ were interpreted by the respective authors as an indication for a link between the isotopic composition of respiration $R_{\mathrm{eco}}^{13}\mathrm{C}$ to the isotopic composition of recent assimilates $\delta^{13}\mathrm{C}_{\mathrm{Ass}}$, which is controlled by photosynthetic discrimination of the heavier $^{13}\mathrm{C}$ according to the Farquhar Model (Farquhar et al., 1989). Thus, in accordance with

10 previous studies, we hypothesize that:

Hypothesis (a): The variability of $R_{\mathrm{eco}}^{13}\mathrm{C}$ can be partly explained by the isotopic composition of recent assimilates $\delta^{13}\mathrm{C}_{\mathrm{Ass}}$, which is controlled by meteorological drivers during photosynthesis according to the Farquhar model. Thus, the variability of $R_{\mathrm{eco}}^{13}\mathrm{C}$ can be linked to the variability of meteorological drivers of photosynthesis and photosynthetic discrimination with a time lag that is consistent with the time lag between respiration and assimilation.

15 To test this hypothesis, we calculated the Pearson correlation coefficient r_{pear} between $R_{\mathrm{eco}}^{13}\mathrm{C}$ and the n-day sum (with n from 1 to 6) of the meteorological quantities that we expect to control $^{13}\mathrm{C}$ discrimination for different time shifts τ. For the time period before the first snow (when the ecosystem was a CO_2 sink), the strongest correlation we found was a moderate negative correlation between $R_{\mathrm{eco}}^{13}\mathrm{C}$ and the two-day-sum of net radiation R_n with a time shift τ of two days (Fig. 8). This correlation is significant with a Pearson correlation coefficient r_{pear} of approximately -0.55, which is clearly beyond the corresponding

20 critical value of approximately $\pm$ 0.38 for N=46 and $\alpha = 0.005$. The time lag of this correlation is in accordance with the expected time lag between assimilation and respiration of two to five days for mature trees (Kuzyakov and Gavrichkova, 2010). But the correlation itself cannot be directly explained by the Farquhar model of discrimination as radiation influences both, the CO_2 supply (by influencing stomatal conductance) and the CO_2 demand (by influencing assimilation) in the leaf (Farquhar and Sharkey, 1982). In particular we did not find a significant time lagged positive correlation between $R_{\mathrm{eco}}^{13}\mathrm{C}$ and

25 VPD, RH or the ratio VPD/PAR (Fig. 8), which could be directly associated with the Farquhar Model and has been found by the above mentioned studies. To test if it might be still reasonable to interpret the observed negative correlation of $R_{\mathrm{eco}}^{13}\mathrm{C}$ with R_n as a time lagged link between $R_{\mathrm{eco}}^{13}\mathrm{C}$ and isotopic composition of recently assimilated material $\delta^{13}\mathrm{C}_{\mathrm{Ass}}$ on ecosystem scale, we performed a more complex calculation of $\delta^{13}\mathrm{C}_{\mathrm{Ass}}$ by using the multilayer model CANVEG, c.f. Sect. 2.8. During the measurement period, the modeled $\delta^{13}\mathrm{C}_{\mathrm{Ass}}$ correlated significantly to the diurnal sum of net radiation R_n with an r_{pear} of

30 0.89 (Fig. 9) - corresponding $r_{\mathrm{crit}} \approx$ 0.33 for N=63. But in contrast to the time lagged correlation we found in our Keeling-Plot data, this correlation is positive (Fig. 9). As the multilayer model does not support the interpretation of the observed negative correlation between R_n and $R_{\mathrm{eco}}^{13}\mathrm{C}$ through the variability of the isotopic composition of recent assimilates $\delta^{13}\mathrm{C}_{\mathrm{Ass}}$, it does not support hypothesis (a).

An alternative interpretation of the observed correlation between the isotopic composition of respiration $R_{\mathrm{eco}}^{13}\mathrm{C}$ and net radiation R_n would be a link between $R_{\mathrm{eco}}^{13}\mathrm{C}$ and the amount of recent assimilates (alternatively to the isotopic composition of recent assimilates). As soil respiration has been measured to account for around 80 % of total respiration in an old beech forest in below 30 km distance to our field site (Knohl et al., 2008), we further focus on soil respiration and discuss the following

5 hypothesis:

Hypothesis (b): The correlation between $R_{\mathrm{eco}}^{13}\mathrm{C}$ and net radiation R_n is not related to differences in discrimination, but rather to differences in the ratio of autotrophic to total soil respiration[1].

A link between photosynthesis and autotrophic soil respiration has been shown in many studies throughout different ecosystems, including a beech dominated forest in less than 30 km air-line distance to our field site in a managed beech forest

10 (Moyano et al., 2008). In this study, the authors found that 73 % of the variability in rhizosphere respiration (the major part of autotrophic soil respiration) correlated with photosynthesis (GPP) and the ratio between autotrophic and total soil respiration was approximately 50 %. Additionally, evidences for a large temporal variability on diurnal and seasonal scale of the contribution of autotrophic to total soil respiration have been reported for a temperate hardwood forest (Savage et al., 2013) and for a mature temperate boreal forest (Carbone et al., 2016). In our field experiment, the observed correlation between $R_{\mathrm{eco}}^{13}\mathrm{C}$ and

15 R_n with an r_{pear} of 0.55 (and thus ($r_{\mathrm{pear}}^2 = 0.3$)) links 30 % of the variability of $R_{\mathrm{eco}}^{13}\mathrm{C}$ to R_n with a time lag of 2-4 days. As the measured isotopic composition of ecosystem respiration $R_{\mathrm{eco}}^{13}\mathrm{C}$ spanned a range of 6 ‰, this corresponds to a range of 1.8 %. Hypothesis (b) would further imply, that this variability over a range of 1.8 ‰ corresponds to that proportion of the variability of autotrophic respiration that is linked to photosynthesis. If we estimate this proportion to represent 73 % of the total variability of autotrophic respiration (following Moyano et al., 2008), the corresponding total variability of autotrophic

20 respiration would correspond to a range of approximately 2.5 ‰. If in autumn the ratio of autotrophic to total respiration would approximate 0 %, this value of 2.5 ‰ would be equal to the difference $\Delta_{\mathrm{tot-aut}} = \delta_{\mathrm{tot}} - \delta_{\mathrm{aut}}$ between the isotopic composition of total respiration δ_{tot} and the isotopic composition of autotrophic respiration δ_{aut}. In general, a value of $\Delta_{\mathrm{tot-aut}} = +2.5$ ‰ is within the range of differences, that have been reviewed to be in average about +4 ‰ (Bowling et al., 2008) for different ecosystems. A positive value of $\Delta_{\mathrm{tot-aut}}$ with a lighter isotopic composition of autotrophic respiration would be consistent

25 to Hypothesis (b). As a note of caution, however, none of the studies that analyze autotrophic soil respiration in the above mentioned review, was performed in a forest ecosystem. For C3 woody species, including forests, more enriched isotopic compositions of autotrophic soil respiration, and thus negative values for $\Delta_{\mathrm{tot-aut}}$, have been reported (Ghashghaie and Badeck, 2014). In a beech forest in Southern Germany, the sign of some involved fractionation effects varied temporally (Paya et al., 2016). Thus, the comparison with literature data about the temporal variability of the ratio between autotrophic and total soil

30 respiration and the respective isotopic compositions gives the possibility that hypothesis (b) is true, but we can, however, not prove it without additional independent measurements.

---

[1]The term 'autotrophic' is not consistently defined among different authors. Here we use this term equivalent to 'root derived respiration', including respiration from the living root tissue, from micro-organisms in the rhizosphere and mycorrhizal symbiotic funghi.

3.2.3 Characteristics of $R_{eco}^{18}O$ and $\delta^{18}O$

The seasonal variability of $\delta^{18}O$ and $R_{eco}^{18}O$ (shown in Fig. 6 and Fig. 7) are influenced by oxygen exchange when CO_2 gets dissolved in different water pools (e.g. leaf and soil water) with variable isotopic compositions. These isotopic compositions in turn, are controlled by multiple physical and biological factors such as temperature, precipitation, vapor pressure deficit (VPD)

5 or the activity of the enzyme carbonic anhydrase, that accelerates the oxygen exchange between water and CO_2, (Miller et al., 1999; Farquhar et al., 1993; Gillon and Yakir, 2000; Bowling et al., 2003a; Wingate et al., 2009). The strongest feature of the measured time series of $R_{eco}^{18}O$ is an approximately 30‰ large decrease within ten days from approximately -15‰ on 8. October to approximately -46‰ on 18. October (Fig. 7). During the same time period, the $\delta^{18}O$ value of nighttime ambient CO_2 in 45 m height decreased from approximately -1‰ down to -3.5‰ at nighttime and down to -6‰ during daytime (Fig.

10 6). As for $R_{eco}^{18}O$, this decrease is the strongest signal in the measured time series of $\delta^{18}O$. The time of these decreases in $R_{eco}^{18}O$ and $\delta^{18}O$ coincided with the time of the first snow and frost event in autumn 2015. This indicates that the snow event has a noticeable effect on both $\delta^{18}O$ and $R_{eco}^{18}O$, but as the change in (nighttime) $R_{eco}^{18}O$ is more than ten times larger than the corresponding change in $\delta^{18}O$ of nighttime CO_2 this effect is particularly enhanced for $R_{eco}^{18}O$.

Possible explanations for the observed large decreases in both $\delta^{18}O$ and $R_{eco}^{18}O$ after the snow would involve the ^{18}O

15 exchange of CO_2 with water pools that are fed by the recent snow event and the response to changes in multiple of the above mentioned physical and biological factors that influence the oxygen exchange between CO_2 and water. One of the factors that can cause a depletion in ^{18}O due to the exchange of oxygen between CO_2 with snow-fed water pools is the fact that snow has in general a lighter isotopic composition than rain. The isotopic composition of rain can often be related to Rayleigh fractionation processes (Gat, 1996) and thus is related to isotopic exchange between the raindrops and air masses in clouds

20 when rain is falling down (Gat, 1996, citing Bolin, 1959 and Friedman et al., 1962). As a result of the continuous isotopic exchange with air masses in the cloud, raindrops do not carry the very depleted isotopic composition within the cloud whereas for snow, the isotopic exchange between the falling snowflakes and the air masses in the cloud does not take place, resulting in a more depleted precipitation (Gat, 1996). As example, Orlowski et al. (2016) reported a maximal difference of approximately 15.5‰ between rain and snow over a two-year measurement period at a field site in approximately 160 km air-line distance

25 from our field site. A smaller maximal difference of approximately 9‰ between snow and the monthly means of the isotopic composition of rain was reported by Wenninger et al. (2011), based on two years of measurements at two catchments in German black forest 414 km air-line distance from our field site. Thus, the depleted isotopic composition of snow compared to rain can explain a part but probably not all of the observed 30‰ decrease in $R_{eco}^{18}O$. One possible additional effect could be the fact that soil respired CO_2 is typically in equilibrium not with rain, but with soil water in the top soil layers (0 to 20 cm) (Miller

30 et al., 1999; Wingate et al., 2009). Evaporative effects can shift the isotopic composition in the upper soil layers towards more enriched values (Miller et al., 1999; Wingate et al., 2009) potentially increasing the $\delta^{18}O$ difference between before and after the snow event.

We tested the correlation between $R_{eco}^{18}O$ and different meteorological variables that potentially control the isotopic composition of different water pools within the ecosystem over the whole measurement period as well as the sub-periods before

and after the first snow (Table 8). As the underlying multiple interaction processes between oxygen in CO_2 and different water pools and the respective isotopic compositions of these pools are complex, this analysis was not performed to causally link the measured $R^{18}_{eco}O$ to a single meteorological driver but rather to look for changes of these correlations that could be interpreted as changes in the processes that drive $R^{18}_{eco}O$ before and after the snow event. For the whole measurement period, the strongest

5 of the analyzed correlations was a correlation between $R^{18}_{eco}O$ and soil moisture at a depth of 8 cm with an R^2 of 0.48 and $p<10^{-9}$. As this correlation becomes insignificant when it is calculated for the periods before and after the snow separately, it can be related to the strong decrease in $R^{18}_{eco}O$ after the snow event that correlates to a rise in soil moisture when the snow melts (Fig. 7). This would be consistent to a heavier isotopic composition in the top soil layers (due to evaporation) before the snow, yielding also higher $\delta^{18}O$ values of $R^{18}_{eco}O$. Also other variables that correlated significantly with $R^{18}_{eco}O$ during the

10 whole measurement period such as soil and air temperatures or shortwave radiation (Table 8) are related to soil evaporation. For the sub-periods before and after the first snow, we found multiple significant correlations with meteorological drivers such as soil and air temperatures, pressure or actual vapor pressure (Table 8). The significant correlations before the first snow become insignificant (or less significant) after the snow and vice versa. This behavior indicates a difference in the processes that drive the ^{18}O isotopic composition of ecosystem respiration $R^{18}_{eco}O$ before and after the snow event.

4 Conclusions

Field-applicable instruments to analyze the isotopic composition of CO_2 have a large potential to be useful for long term measurement setups on meteorological towers and networks such as ICOS https://www.icos-ri.eu/ or NEON http://www.neonscience.org/ to deliver new insights into the carbon cycle. The new Isotope Ratio Infrared Spectrometer (IRIS) Delta Ray used in this study provides an opportunity to measure the CO_2 concentration c and its isotopic compositions $\delta^{13}C$

20 and $\delta^{18}O$ with limited maintenance effort at remote sites. Here, we successfully demonstrate the field applicability of the Delta Ray IRIS, which we used to measure c, $\delta^{13}C$ and $\delta^{18}O$ in a managed beech forest for three months in autumn 2015. The Delta Ray IRIS implemented here with the instrument's internal calibration, showed adequate precision, accuracy and long-term stability to perform robust measurements of c, $\delta^{13}C$ and $\delta^{18}O$ in air in our continuous setup. The easy operation of the automatically calibrated Delta Ray IRIS allowed us to measure seasonal variability of the isotopic composition of night-

25 time CO_2 exchange based on Keeling-Plots. The strong effect of the first frost and snow event on both the $\delta^{13}C$ and $\delta^{18}O$ of nighttime CO_2 exchange indicates that singular events, even if short, may strongly influence the isotopic imprint of terrestrial ecosystems on atmospheric CO_2.

5 Code availability

An earlier version of the multilayer model CANVEG can be found here:

30   https://nature.berkeley.edu/biometlab/BiometWeb/canoak_V2.c

6 Data availability

All data used for the figures presented here is provided in the supplementary material.

7 Appendices

- Appendix A: Measures to improve data quality

5 *Author contributions.* The authors contributed to this paper in the following ways: The experimental setup in the field and data processing were carried out, discussed and interpreted by Jelka Braden-Behrens and Alexander Knohl. The validation of and simulations with the multilayer model CANVEG (Sect. 2.8) were performed, discussed and interpreted by Yuan Yan, Jelka Braden-Behrens and Alexander Knohl. All authors proof-read and commented on the paper.

8 Competing interests

10 We declare that we have no conflict of interest. However, we borrowed the instrument at no cost from *Thermo Scientific*, Waltham, USA, to perform instrument tests and to use the instrument under field conditions and Jelka Braden-Behrens and Alexander Knohl published a short (not peer reviewed) technical paper (Braden-Behrens et al., 2017) together with HJ Jost and Magda Mandic, who were both working for *Thermo Scientific*, when we borrowed the instrument. This not peer reviewed technical paper also briefly describes our experimental setup and discusses instrument performance.

15 *Acknowledgements.* This project was partly funded by the Dorothea-Schlözer-Fellowship and by the German Research Foundation (DFG, project ISOFLUXES KN 582/7-1). The work was partially supported by the European Research Council under the European Union's Horizon 2020 research and innovation programme (grant agreement n. 682512 – OXYFLUX). We thank *Thermo Scientific*, Waltham, USA, to borrow us the instrument for free and in particular HJ Jost and Magda Mandic for their advice and support especially concerning how to set up and operate the Delta Ray analyzer. The technicians of the bioclimatology group of the University of Goettingen, especially Dietmar Fellert 20 Frank Tiedemann and Edgar Tunsch as well as the student assistant Elke Schäpermeier helped substantially with the experimental setup and maintenance. We thank Yakov Kuzyakov, Lydia Gentsch and Mattia Bonazza for their remarks on data interpretation. Additionally we thank the forest manager Ulrich Breitenstein for allowing the experimental setup at this site.

References

Affek, H. and Yakir, D.: The stable isotopic composition of atmospheric CO_2, in: Treatise on geochemistry, edited by Holland, H. and Turekian, K., vol. 5, chap. 5.7, pp. 179–212, Elsevier, 2 edn., doi:10.1016/B978-0-08-095975-7.00407-1, 2014.

Anthoni, P., Knohl, A., Rebmann, C., Freibauer, A., Mund, M., Ziegler, W., Kolle, O., and Schulze, E. D.: Forest and agricultural land-use-
5   dependent CO_2 exchange in Thuringia, Germany, Glob. Change Biol., 10, 2005–2019, doi:10.1111/j.1365-2486.2004.00863.x, 2004.

Baldocchi, D. D.: Measuring and modelling carbon dioxide and water vapour exchange over a temperate broad-leaved forest during the 1995 summer drought, Plant, Cell Environ., 20, 1108–1122, doi:10.1046/j.1365-3040.1997.d01-147.x, 1997.

Baldocchi, D. D. and Bowling, D. R.: Modelling the discrimination of $^{13}CO_2$ above and within a temperate broad-leaved forest canopy on hourly to seasonal time scales, Plant, Cell Environ., 26, 231–244, doi:10.1046/j.1365-3040.2003.00953.x, 2003.

10   Baldocchi, D. D. and Wilson, K. B.: Modelling CO_2 and water vapor exchange of a temperate broadleaved forest across hourly to decadal time scales, Ecol. Model., 142, 155–184, doi:10.1016/S0304-3800(01)00287-3, 2001.

Baldocchi, D. D., Vogel, C. A., and Hall, B.: Seasonal variation of carbon dioxide exchange rates above and below a boreal jack pine forest, Agr. Forest Meteorol., 83, 147–170, doi:10.1016/S0168-1923(96)02335-0, 1997.

Baldocchi, D. D., Fuentes, J. D., Bowling, D. R., Turnipseed, A. A., and Monson, R. K.: Scaling isoprene fluxes from leaves to
15   canopies: Test cases over a boreal aspen and a mixed species temperate forest, J. Appl. Meteorol., 38, 885–898, doi:10.1175/1520-0450(1999)038<0885:SIFFLT>2.0.CO;2, 1999.

Baldocchi, D. D., Wilson, K. B., and Gu, L.: How the environment, canopy structure and canopy physiological functioning influence carbon, water and energy fluxes of a temperate broad-leaved deciduous forest - An assessment with the biophysical model CANOAK., Tree Physiol., 22, 1065–1077, doi:10.1093/treephys/22.15-16.1065, 2002.

20   Barbour, M. M., Hunt, J. E., Kodama, N., Laubach, J., McSeveny, T. M., Rogers, G. N. D., Tcherkez, G., and Wingate, L.: Rapid changes in $\delta^{13}C$ of ecosystem-respired CO_2 after sunset are consistent with transient ^{13}C enrichment of leaf respired CO_2, New Phytol., 190, 990–1002, doi:10.1111/j.1469-8137.2010.03635.x, 2011.

Bolin, B.: On the use of tritium as a tracer for water in nature, in: Proceedings of the 2nd conference on the peaceful uses of atomic energy, pp. 18:336–44, UN, Geneva, 1959.

25   Bowling, D. R., Tans, P. P., and Monson, R. K.: Partitioning net ecosystem carbon exchange with isotopic fluxes of CO_2, Glob. Change Biol., 7, 127–145, doi:10.1046/j.1365-2486.2001.00400.x, 2001.

Bowling, D. R., McDowell, N. G., Bond, B. J., Law, B. E., and Ehleringer, J. R.: ^{13}C content of ecosystem respiration is linked to precipitation and vapor pressure deficit, Oecologia, 131, 113–124, doi:10.1007/s00442-001-0851-y, 2002.

Bowling, D. R., McDowell, N. G., Welker, J. M., Bond, B. J., Law, B. E., and Ehleringer, J. R.: Oxygen isotope content of CO_2 in noc-
30   turnal ecosystem respiration: 2. Short-term dynamics of foliar and soil component fluxes in an old-growth ponderosa pine forest, Global Biogeochem. Cy., 17, GB2082, doi:10.1029/2003GB002082, 2003a.

Bowling, D. R., McDowell, N. G., Welker, J. M., Bond, B. J., Law, B. E., and Ehleringer, J. R.: Oxygen isotope content of CO_2 in nocturnal ecosystem respiration: 1. Observations in forests along a precipitation transect in Oregon, USA, Global Biogeochem. Cy., 17, 3101–3114, doi:10.1029/2003GB002081, 2003b.

35   Bowling, D. R., Sargent, S. D., Tanner, B. D., and Ehleringer, J. R.: Tunable diode laser absorption spectroscopy for stable isotope studies of ecosystem-atmosphere CO_2 exchange, Agr. Forest Meteorol., 118, 1–19, doi:10.1016/S0168-1923(03)00074-1, 2003c.

Bowling, D. R., Burns, S. P., Conway, T. J., Monson, R. K., and White, J. W. C.: Extensive observations of CO_2 carbon isotope content in and above a high-elevation subalpine forest, Global Biogeochem. Cy., 19, GB3023, doi:10.1029/2004GB002394, 2005.

Bowling, D. R., Pataki, D. E., and Randerson, J. T.: Carbon isotopes in terrestrial ecosystem pools and CO_2 fluxes, New Phytol., 178, 24–40, doi:10.1111/j.1469-8137.2007.02342.x, 2008.

5 Braden-Behrens, J., Knohl, A., Jost, H.-J., and Mandic, M.: Measuring the isotopic composition of ecosystem respiration in a temperate beech forest, Thermo Scientific White Paper, p. WP30385, https://tools.thermofisher.com/content/sfs/brochures/WP-30385-IRIS-Isotopic-Composition-Respiration-Beech-WP30385-EN.pdf, 2017.

Carbone, M. S., Richardson, A. D., Chen, M., Davidson, E. A., Hughes, H., Savage, K. E., and Hollinger, D. Y.: Constrained partitioning of autotrophic and heterotrophic respiration reduces model uncertainties of forest ecosystem carbon fluxes but not stocks, J. Geophys.

10 Res.-Biogeo., 121, 2476–2492, doi:10.1002/2016JG003386, 2016.

Davis, S. P., Abrams, M. C., and Brault, J. W.: Fourier transform spectrometry, Academic Press, 2001.

Ekblad, A. and Högberg, P.: Natural abundance of ^{13}C in CO_2 respired from forest soils reveals speed of link between tree photosynthesis and root respiration, Oecologia, 127, 305–308, doi:10.1007/s004420100667, 2001.

Esler, M. B., Griffith, D. W. T., Wilson, S. R., and Steele, L. P.: Precision trace gas analysis by FT-IR spectroscopy. 2. The ^{13}C/^{12}C isotope

15 ratio of CO_2, Anal. Chem., 72, 216–221, doi:10.1021/ac990563x, 2000.

Farquhar, G. D. and Sharkey, T. D.: Stomatal conductance and photosynthesis, Annu. Rev. Plant Physiol., 33, 317–345, doi:10.1146/annurev.pp.33.060182.001533, 1982.

Farquhar, G. D., Ehleringer, J. R., and Hubick, K. T.: Carbon isotope discrimination and photosynthesis, Annu. Rev. Plant Phys., 40, 503–537, doi:10.1146/annurev.pp.40.060189.002443, 1989.

20 Farquhar, G. D., Lloyd, J., Taylor, J. A., Flanagan, L. B., Syvertsen, J. P., Hubick, K. T., Wong, S. C., and Ehleringer, J. R.: Vegetation effects on the isotope composition of oxygen in atmospheric CO_2, Nature, 363, 439–443, doi:10.1038/363439a0, 1993.

Flanagan, L. B. and Ehleringer, J. R.: Ecosystem–atmosphere CO_2 exchange: interpreting signals of change using stable isotope ratios, Trends Ecol. Evol., 13, 10–14, doi:10.1016/S0169-5347(97)01275-5, 1998.

Friedman, I., Machta, L., and Soller, R.: Water-vapor exchange between a water droplet and its environment, J. Geophys. Res., 67, 2761–

25 2766, doi:10.1029/JZ067i007p02761, 1962.

Gat, J. R.: Oxygen and hydrogen isotopes in the hydrologic cycle, Annu. Rev. Earth Pl. Sc., 24, 225–262, doi:10.1146/annurev.earth.24.1.225, 1996.

Geldern, R. V., Nowak, M. E., Zimmer, M., Szizybalski, A., Myrttinen, A., Barth, J. A. C., and Jost, H.-J.: Field-based stable isotope analysis of carbon dioxide by mid-infrared laser spectroscopy for carbon capture and storage monitoring, Anal. Chem., 86, 12 191–12 198,

30 doi:10.1021/ac5031732, 2014.

Ghashghaie, J. and Badeck, F. W.: Opposite carbon isotope discrimination during dark respiration in leaves versus roots - a review, New Phytol., 201, 751–769, doi:10.1111/nph.12563, 2014.

Gillon, J. S. and Yakir, D.: Naturally low carbonic anhydrase activity in C_4 and C_3 plants limits discrimination against $C^{18}OO$ during photosynthesis, Plant, Cell Environ., 23, 201–213, doi:10.1046/j.1365-3040.2000.00597.x, 2000.

35 Griffis, T. J.: Tracing the flow of carbon dioxide and water vapor between the biosphere and atmosphere: A review of optical isotope techniques and their application, Agr. Forest Meteorol., 174-175, 85–109, doi:10.1016/j.agrformet.2013.02.009, 2013.

Griffith, D. W. T., Deutscher, N. M., Caldow, C., Kettlewell, G., Riggenbach, M., and Hammer, S.: A Fourier transform infrared trace gas and isotope analyser for atmospheric applications, Atmos. Meas. Tech., 5, 2481–2498, doi:10.5194/amt-5-2481-2012, 2012.

Griffiths, P. R., De Haseth, J. A., and Winefordner, J. D.: Fourier transform infrared spectrometry, Chemical analysis: A series of monographs on analytical chemistry and its applications, Wiley, 2007.

Guillon, S., Pili, E., and Agrinier, P.: Using a laser-based CO_2 carbon isotope analyser to investigate gas transfer in geological media, Appl. Phys. B-Lasers O., 107, 449–457, doi:10.1007/s00340-012-4942-8, 2012.

International Atomic Energy Agency: Reference and intercomparison materials for stable isotopes of light elements, in: Proceedings of a consultants meeting, edited by IAEA, pp. IAEA–TECDOC–825, Vienna, 1995.

Keeling, C. D.: The concentration and isotopic abundances of atmospheric carbon dioxide in rural areas, Geochim. Cosmochim. Ac., 13, 322–334, doi:10.1016/0016-7037(58)90033-4, 1958.

Kerstel, E. and Gianfrani, L.: Advances in laser-based isotope ratio measurements: Selected applications, Appl. Phys. B-Lasers O., 92, 439–449, doi:10.1007/s00340-008-3128-x, 2008.

Knohl, A. and Baldocchi, D. D.: Effects of diffuse radiation on canopy gas exchange processes in a forest ecosystem, J. Geophys. Res., 113, G02 023, doi:10.1029/2007JG000663, 2008.

Knohl, A. and Buchmann, N.: Partitioning the net CO_2 flux of a deciduous forest into respiration and assimilation using stable carbon isotopes, Global Biogeochem. Cy., 19, GB4008, doi:10.1029/2004GB002301, 2005.

Knohl, A., Werner, R. A., Brand, W. A. ., and Buchmann, N.: Short-term variations in ^{13}C of ecosystem respiration reveals link between assimilation and respiration in a deciduous forest, Oecologia, 142, 70–82, doi:10.1007/s00442-004-1702-4, 2005.

Knohl, A., Søe, A. R. B., Kutsch, W. L., Göckede, M., and Buchmann, N.: Representative estimates of soil and ecosystem respiration in an old beech forest, Plant Soil, 302, 189–202, doi:10.1007/s11104-007-9467-2, 2008.

Kuzyakov, Y. and Gavrichkova, O.: Review: Time lag between photosynthesis and carbon dioxide efflux from soil: A review of mechanisms and controls, Glob. Change Biol., 16, 3386–3406, doi:10.1111/j.1365-2486.2010.02179.x, 2010.

Miller, J. B., Yakir, D., White, J. W. C., and Tansl, P. P.: Measurement of $^{18}O/^{16}O$ in the soil-atmosphere CO_2 flux, Global Biogeochem. Cy., 13, 761–774, doi:10.1029/1999GB900028, 1999.

Mohn, J., Werner, R. A., Buchmann, B., and Emmenegger, L.: High-precision $\delta^{13}CO_2$ analysis by FTIR spectroscopy using a novel calibration strategy, J. Mol. Struct., 834-836, 95–101, doi:10.1016/j.molstruc.2006.09.024, 2007.

Moyano, F. E., Kutsch, W. L., and Rebmann, C.: Soil respiration fluxes in relation to photosynthetic activity in broad-leaf and needle-leaf forest stands, Agr. Forest Meteorol., 148, 135–143, doi:10.1016/j.agrformet.2007.09.006, 2008.

Mund, M.: Carbon pools of European beech forests (Fagus sylvatica) under different silvicultural management, Berichte des Forschungszentrums Waldökosysteme Reihe A, Band 189, 1–256, 2004.

Ogée, J., Peylin, P., Ciais, P., Bariac, T., Brunet, Y., Berbigier, P., Roche, C., Richard, P., Bardoux, G., and Bonnefond, J.-M.: Partitioning net ecosystem carbon exchange into net assimilation and respiration using $^{13}CO_2$ measurements: A cost-effective sampling strategy, Global Biogeochem. Cy., 17, 3901–3916, doi:10.1029/2002GB001995, 2003.

Oikawa, P., Sturtevant, C., Knox, S. H., Verfaillie, J., Huang, Y.-W., and Baldocchi, D. D.: Revisiting the partitioning of net ecosystem exchange of CO_2 into photosynthesis and respiration with simultaneous flux measurements of $^{13}CO_2$ and CO_2, soil respiration and a biophysical model, CANVEG, Agr. Forest Meteorol., 234-235, 149–163, doi:10.1016/j.agrformet.2016.12.016, 2017.

Orlowski, N., Kraft, P., Pferdmenges, J., and Breuer, L.: Exploring water cycle dynamics by sampling multiple stable water isotope pools in a developed landscape in Germany, Hydrol. Earth Syst. Sc., 20, 3873–3894, doi:10.5194/hess-20-3873-2016, 2016.

Pataki, D. E., Ehleringer, J. R., Flanagan, L. B., Yakir, D., Bowling, D. R., Still, C., Buchmann, N., Kaplan, J. O., and Berry, J. A.: The application and interpretation of Keeling plots in terrestrial carbon cycle research, doi:10.1029/2001GB001850, 2003.

Paya, A. M., Grams, T. E. E., and Bauerle, T. L.: Seasonal dynamics of δ^{13}C of C-rich fractions from Picea abies (Norway spruce) and Fagus sylvatica (European beech) fine roots, Plant, Cell Environ., 39, 2004–2013, doi:10.1111/pce.12765, 2016.

Savage, K., Davidson, E. A., and Tang, J.: Diel patterns of autotrophic and heterotrophic respiration among phenological stages, Glob. Change Biol., 19, 1151–1159, doi:10.1111/gcb.12108, 2013.

5   Sturm, P., Eugster, W., and Knohl, A.: Eddy covariance measurements of CO_2 isotopologues with a quantum cascade laser absorption spectrometer, Agr. Forest Meteorol., 152, 73–82, doi:10.1016/j.agrformet.2011.09.007, 2012.

Thermo Fisher Scientific: Delta Ray^{TM} Isotope ratio infrared spectrometer: Operating manual, Thermo Scientific, Bremen, 2014.

Thomson, J. J.: Rays of positive electricity, Nature, 79, 52–56, doi:10.1038/079052a0, 1908.

Vardag, S. N., Hammer, S., Sabasch, M., Griffith, D. W. T., and Levin, I.: First continuous measurements of δ^{18}O-CO_2 in air with a Fourier
10   transform infrared spectrometer, Atmos. Meas. Tech., 8, 579–592, doi:10.5194/amt-8-579-2015, 2015.

Vogel, F. R., Huang, L., Ernst, D., Giroux, L., Racki, S., and Worthy, D. E. J.: Evaluation of a cavity ring-down spectrometer for in situ observations of $^{13}CO_2$, Atmos. Meas. Tech., 6, 301–308, doi:10.5194/amt-6-301-2013, 2013.

Wehr, R., Munger, J., Nelson, D., McManus, J., Zahniser, M., Wofsy, S., and Saleska, S.: Long-term eddy covariance measurements of the isotopic composition of the ecosystem–atmosphere exchange of CO_2 in a temperate forest, Agr. Forest Meteorol., 181, 69–84,
15   doi:10.1016/j.agrformet.2013.07.002, 2013.

Wehr, R., Munger, J. W., McManus, J. B., Nelson, D. D., Zahniser, M. S., Davidson, E. A., Wofsy, S. C., and Saleska, S. R.: Seasonality of temperate forest photosynthesis and daytime respiration, Nature, 534, 680–683, doi:10.1038/nature17966, 2016.

Wenninger, J., Koeninger, P., and Schneider, P.: Isotopic characterization of snow variability in two mountainous catchments, black forest mountains, Germany, in: International symposium on water resource and environmental protection (ISWREP), pp. 1004–1007, 2011.

20   Werle, P. W.: Diode-laser sensors for in-situ gas analysis, in: Laser in environmental and life sciences: Modern analytical methods, edited by Hering, P., Lay, J. P., and Stry, S., pp. 223–243, Springer, Berlin, Heidelberg, doi:10.1007/978-3-662-08255-3_11, 2004.

Werner, C., Schnyder, H., Cuntz, M., Keitel, C., Zeeman, M. J., Dawson, T. E., Badeck, F. W., Brugnoli, E., Ghashghaie, J., Grams, T. E. E., Kayler, Z. E., Lakatos, M., Lee, X., Máguas, C., Ogée, J., Rascher, K. G., Siegwolf, R. T. W., Unger, S., Welker, J. M., Wingate, L., and Gessler, A.: Progress and challenges in using stable isotopes to trace plant carbon and water relations across scales, Biogeosciences, 9,
25   3083–3111, doi:10.5194/bg-9-3083-2012, 2012.

Wingate, L., Ogée, J., Cuntz, M., Genty, B., Reiter, I., Seibt, U., Yakir, D., Maseyk, K., Pendall, E. G., Barbour, M. M., Mortazavi, B., Burlett, R., Peylin, P., Miller, J., Mencuccini, M., Shim, J. H., Hunt, J., and Grace, J.: The impact of soil microorganisms on the global budget of δ^{18}O in atmospheric CO_2, Proceedings of the National Academy of Sciences, 106, 22 411–22 415, doi:10.1073/pnas.0905210106, 2009.

Yakir, D. and Wang, X.-F.: Fluxes of CO_2 and water between terrestrial vegetation and the atmosphere estimated from isotope measurements,
30   Nature, 380, 515–517, 1996.

Yakir, D., da Silveira, L., and Sternberg, L.: The use of stable isotopes to study ecosystem gas exchange, Oecologia, 123, 297–311, doi:10.1007/s004420051016, 2000.

Zhang, J., Griffis, T. J., and Baker, J. M.: Using continuous stable isotope measurements to partition net ecosystem CO_2 exchange, Plant, Cell Environ., 29, 483–496, doi:10.1111/j.1365-3040.2005.01425.x, 2006.

35   Zobitz, J., Keener, J., Schnyder, H., and Bowling, D. R.: Sensitivity analysis and quantification of uncertainty for isotopic mixing relationships in carbon cycle research, Agr. Forest Meteorol., 136, 56–75, doi:10.1016/j.agrformet.2006.01.003, 2006.
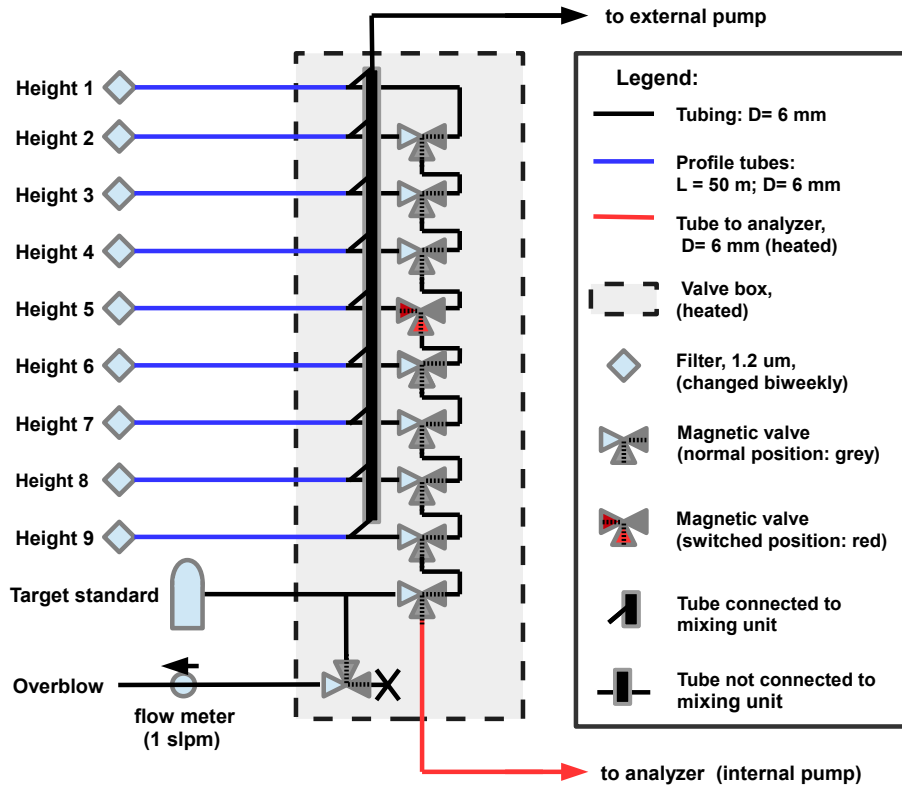
Figure 1. Plumbing scheme for the measurements of nine heights and a target standards, the example shows the valve positions when height 5 is sampled
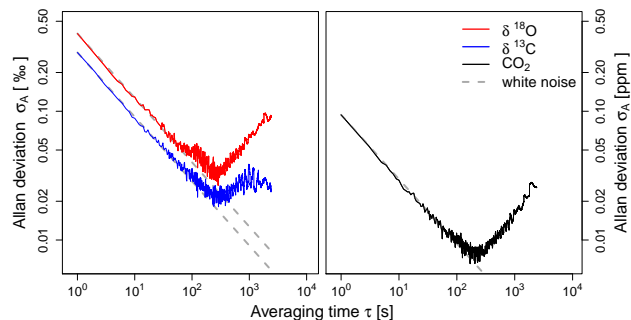
Figure 2. Allan deviation σ_A in ‰ VPDB for ^{13}C; in ‰ VPDB-CO2 for ^{18}O and in ppm for CO_2 concentration, solid lines show the calculated Allan deviation and the dashed line shows the typical white frequency noise error scaling.
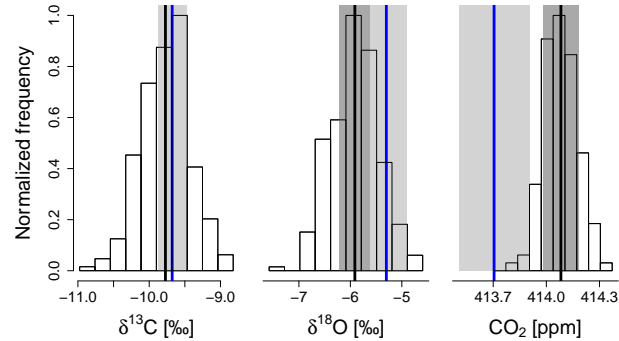
Figure 3. Frequency distributions of 300 measurements (each 1 s long) of a gas tank with pressurized air with known concentration and δ values ('PA-tank', c.f. Table 3).The black lines mark the respective means of all measurements and the area shaded in dark gray shows the expected uncertainty range based on the uncertainties of calibration tanks (only 0.01 ‰ for δ^{13}C, thus not visible on this scale). The blue lines show the values that were measured with an independently calibrated instrument at the field site with their corresponding uncertainties in light gray.
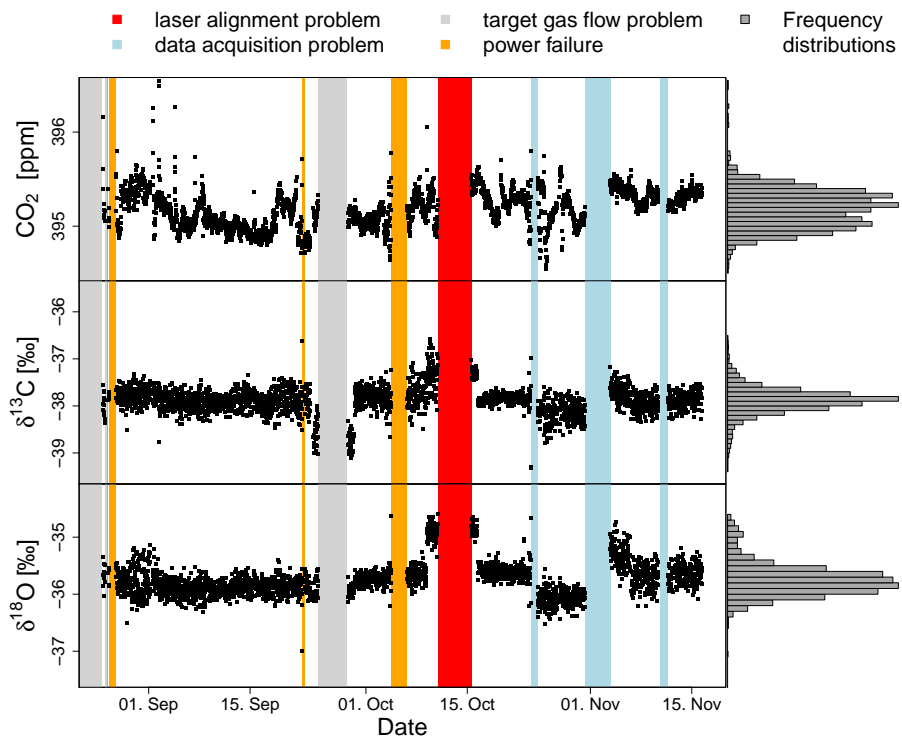
Figure 4. Time series and frequency distributions of half-hourly performed measurements of the concentration (top panel) and δ values (middle and bottom panel) for target gas 'SA-CO2-5' (c.f. Table 3) for the whole measurement period. Major reasons for data gaps are marked with different colors.
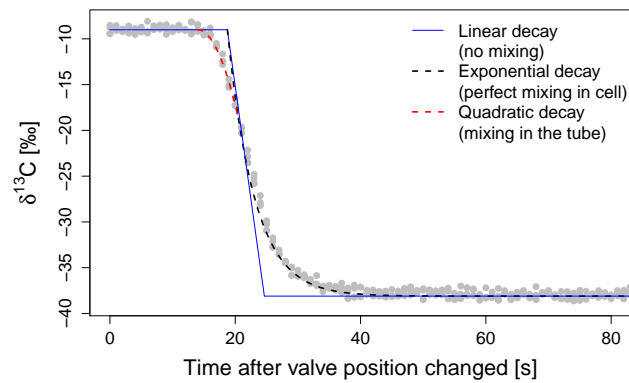
Figure 5. The turnover behavior of our experimental setup can be divided into three phases with different dominant turnover mechanisms: Directly after switching it took approximately 14 s to flush the tubing, the adjacent 4 s were dominated by the mixing processes in the tubes before the gas entered the measuring cell (quadratic fit) and finally we observed a turnover behavior that is dominated by mixing processes within the measuring cell (exponential fit) with a characteristic decay time of $\tau_{10\%} = 10$ s for δ^{13}C. The turnover was similar for δ^{18}O (not shown).
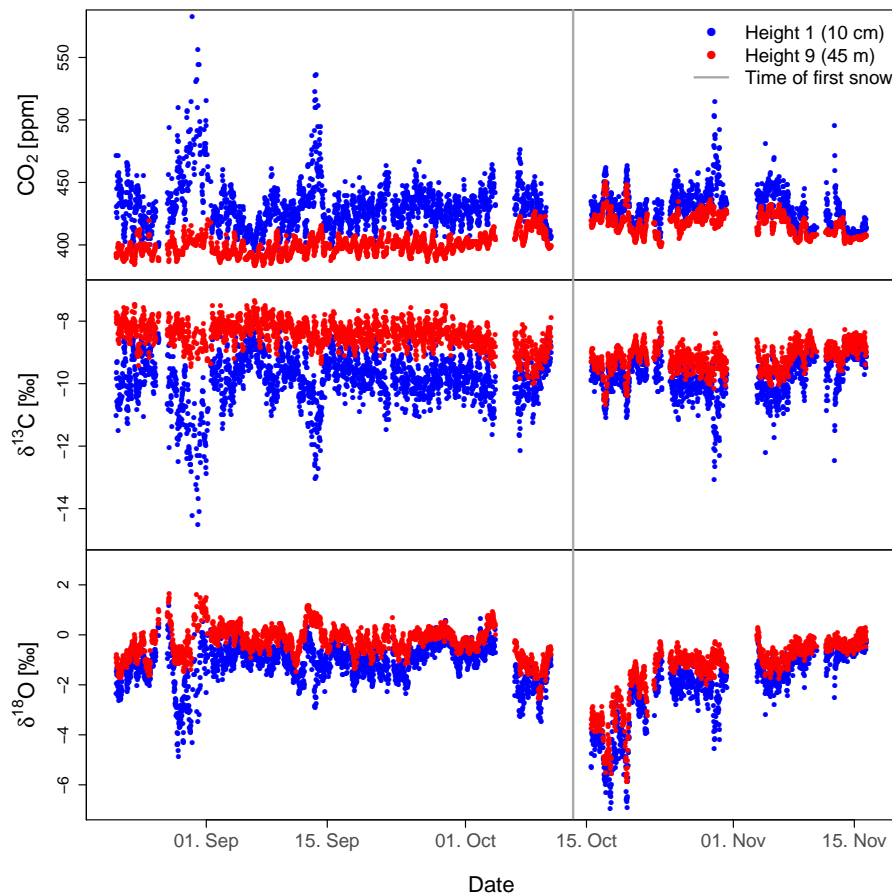
Figure 6. Time series of all measured concentrations c and both δ values at the lowest (blue points) and highest (red points) inlet in 0.1 respectively 45 m height.
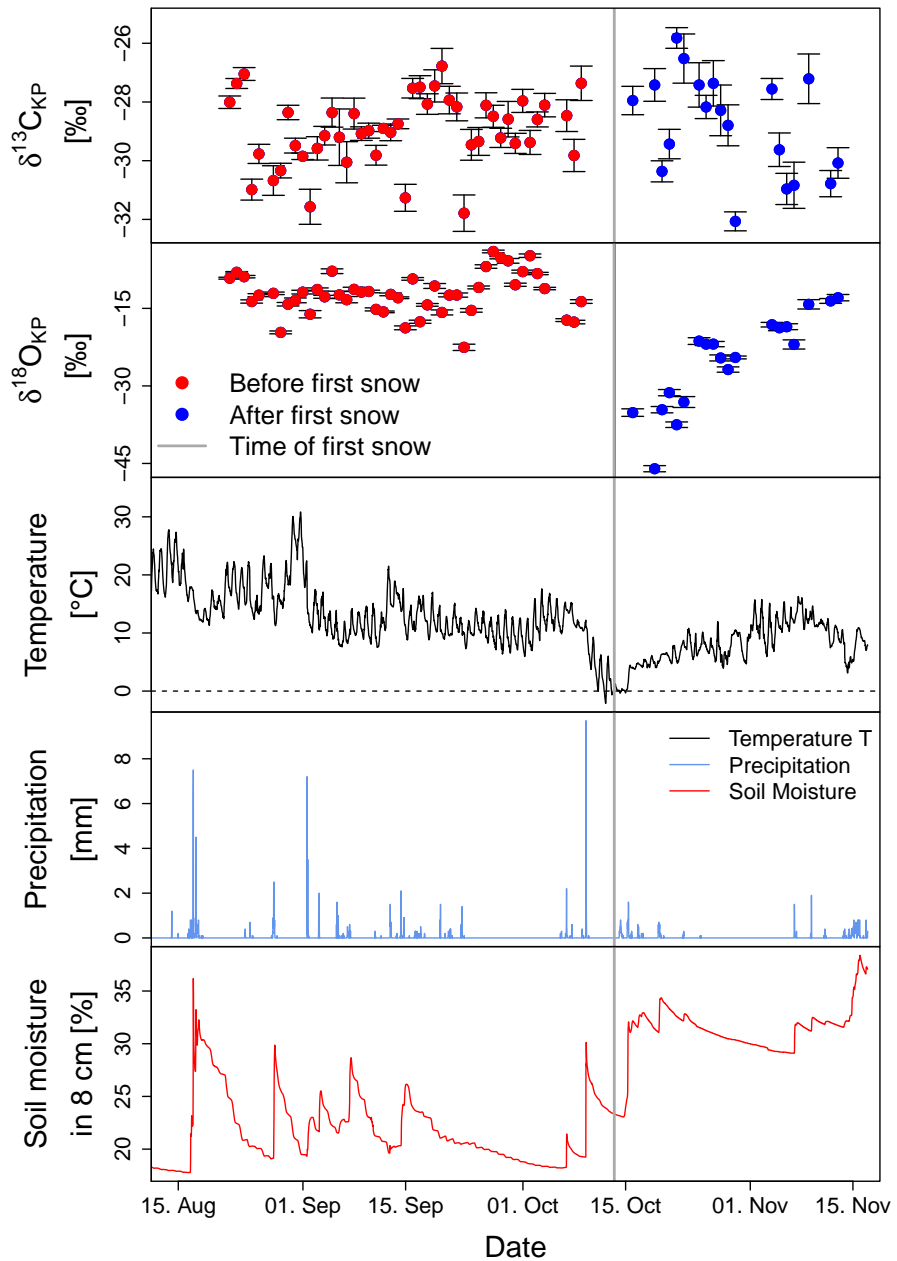
Figure 7. Time series of the measured nighttime Keeling-Plot intercepts $\delta^{13}C_{KP}$ and $\delta^{18}O_{KP}$ in combination with temperature, precipitation and soil moisture in 8 cm depth. Error bars denote the standard error of the Keeling-Plot intercept (based on the linear regression of δ vs. $1/c$). A particular feature of this time series is a first snow and frost event on 13. October 2015, marked in gray.
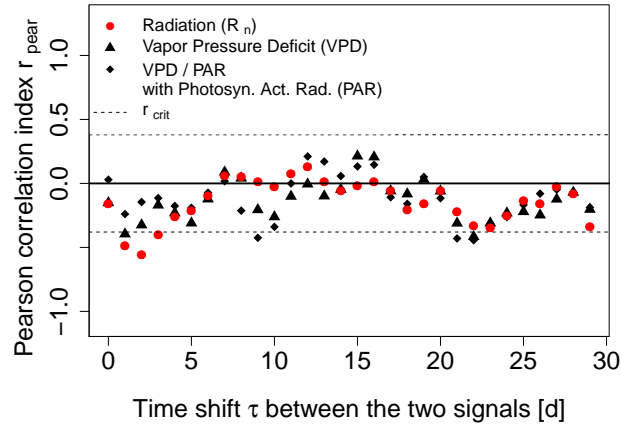
Figure 8. The Pearson correlation coefficient of nighttime $\delta^{13}C_{KP}$ and the two-day-sum of different meteorological variables (shifted by different times τ) before the first snow event in autumn 2015. Error bars denote the standard error of the Keeling-Plot intercept (based on the linear regression of δ vs. $1/c$).
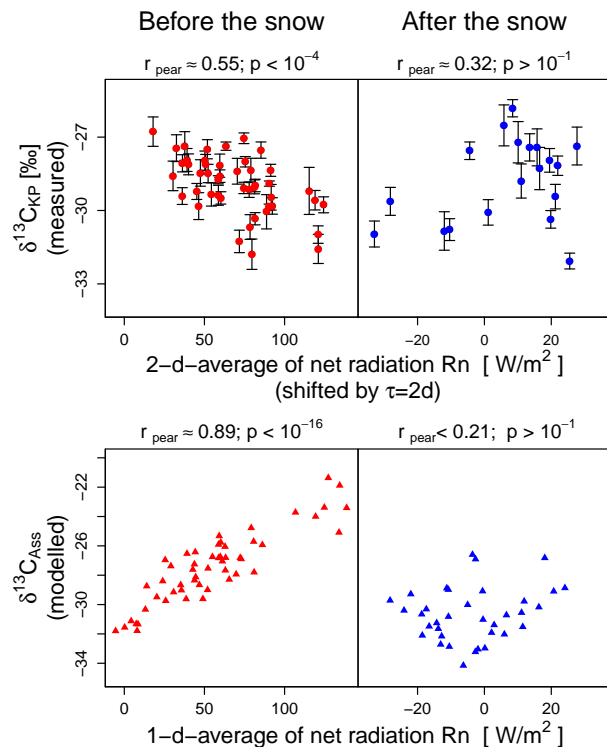
Figure 9. Observed relationships between net radiation R_n and the measured nighttime Keeling-Plot intercepts $\delta^{13}C_{KP}$ (top panels) and the modeled ^{13}C composition of assimilated material $\delta^{13}C_{Ass}$ (bottom panels). Significant correlations were observed before the first snow (left) but became insignificant after the snow (right). r_{pear} and p values are derived from the respective linear regressions.

Table 1. Nomenclature and abbreviations used in this publication, numbers for reference standards R_{std} from International Atomic Energy Agency (1995)

	Stable isotope specific nomenclature
R_{std}	Isotope ratio $C_{\text{heavy}}/C_{\text{light}}$ of an (arbitrary) reference standard
δ value	Relative deviation of the measured isotope ratio from R_{std}
VPDB	Vienna Pee Dee Belemnite - standard for ^{13}C ($R_{VPDB} \approx 0.01124$)
VPDB-CO2	Vienna Pee Dee Belemnite - standard for ^{18}O ($R_{VPDB-CO2} \approx 0.0020883$)
	Nomenclature
σ_A	Allan deviation
R_n	Net radiation
RH	Relative humidity
VPD	Vapor pressure deficit
δ_{KP}	Keeling-Plot intercept
R_{eco}	Isotopic composition of respiration, integrated over the ecosystem
	Technical abbreviations
IRIS	Isotope Ratio Infrared Spectrometer
IRMS	Isotope Ratio Mass Spectrometer
OA-ICOS	Off-axis Integrated Cavity Output Spectroscopy
CRDS	Cavity Ring Down Spectroscopy

Table 2. Examples for different optical instruments that measure the isotopic composition of CO_2 and reported values for minimal Allan deviations σ_A and the corresponding averaging times $\tau_{\min}$ (if available), see also Table 2 of the review of Griffis (2013).

1. Broadband light source based instruments

Instrument:	Fourier Transform Infrared Spectrometer: Spectronus analyzer, *Ecotech Pty Ltd., Australia*
Minimal Allan deviation for δ^{13}C :	$\sigma_A(\tau_{\min} \approx 100\,\text{m})=0.01\,$‰ (Griffith et al., 2012)
Minimal Allan deviation for δ^{18}O :	$\sigma_A(\tau_{\min} \approx 120\,\text{m})=0.1\,$‰ (Vardag et al., 2015)

Instrument:	Fourier Transform Infrared Spectrometer: Nicolet Avatar, *Thermo Electron, USA*
Minimal Allan deviation for δ^{13}C :	$\sigma_A(\tau_{\min} \approx 16\,\text{m})=0.15\,$‰ (Mohn et al., 2007)

2. a) Direct laser absorption spectrometers in mid infrared

Instrument:	Quantum cascade laser absorption spectrometer: CCIA-48, *Los Gatos Research Inc., USA*
Minimal Allan deviation for δ^{13}C :	$\sigma_A(\tau_{\min} \approx 300\,\text{s})=0.06\,$‰ (Oikawa et al., 2017)
Minimal Allan deviation for δ^{18}O :	$\sigma_A(\tau_{\min} \approx 300\,\text{s})=0.04\,$‰ (Oikawa et al., 2017)

Instrument:	Quantum cascade laser absorption spectrometer: QCLAS *Aerodyne Research Inc., USA*
Minimal Allan deviation for δ^{13}C :	$\sigma_A(\tau_{\min} \approx 100\,\text{s})=0.01\,$‰ (Wehr et al., 2013); $\sigma_A(\tau_{\min} \approx 100\,\text{s})=0.06\,$‰ (Sturm et al., 2012)
Minimal Allan deviation for δ^{18}O :	$\sigma_A(\tau_{\min} \approx 100\,\text{s})=0.06\,$‰ (Sturm et al., 2012)

Instrument:	Lead-salt tunable diode laser absorption spectrometer: TGA100A/200, *Campbell Scientific Inc., USA*
Minimal Allan deviation:	no data for minimal σ_A, ideal averaging time $\tau_{\min} \approx 30\,$s (Bowling et al., 2003c)
High frequency Allan deviation:	$\sigma_A(\tau=0.1\,\text{s})=1.5\,$‰ for δ^{13}C and 2.2‰ for δ^{18}O (Bowling et al., 2003c)

Instrument:	Isotope Ratio Infrared Spectrometer: Delta Ray, *Thermo Scientific Inc., USA*
Minimal Allan deviation for δ^{13}C :	$\sigma_A(\tau_{\min} \approx 500\,s)=0.04\,$‰ (Geldern et al., 2014); $\sigma_A(\tau_{\min} \approx 300\,s)=0.02\,$‰ (this study, table 5)
Minimal Allan deviation for δ^{18}O :	$\sigma_A(\tau_{\min} \approx 300\,s)=0.04\,$‰ (this study, table 5)

2. b) Laser absorption spectrometers in near infrared

Instrument:	Cavity Ringdown Spectrometer: G1101-i and G1101-i+, *Picarro Inc., USA*
Minimal Allan deviation for δ^{13}C :	$\sigma_A(\tau_{\min} \approx 60\,\text{min}) \leq 0.1\,$‰ (Vogel et al., 2013)

Instrument:	Off-Axis Integrated Cavity Output Spectrometer: CCIA DLT-100, *Los Gatos Research Inc., USA*
Minimal Allan deviation for δ^{13}C :	$\sigma_A(\tau_{\min} \approx 200\,\text{s})=0.04\,$‰ (at app. 20 000 ppm CO_2) (Guillon et al., 2012); $\sigma_A(\tau_{\min} \approx 200\,\text{s})=0.6\,$‰ (at app. 2 000 ppm CO_2) (Guillon et al., 2012)

Table 3. Known CO_2-concentrations c and δ values for gas tanks used for calibration and instrument performance measurements. All measured concentrations and δ values refer to measurements that were done at Max-Planck Institute for Biogeochemistry in Jena, except the PA-tank that was measured by an independently calibrated quantum-cascade laser based absorption spectrometer (QCLAS, Aerodyne Research, Inc, Boston, USA) at the field site and the δ^{13}C-values of the two pure CO_2 tanks. The latter values were measured with IRMS at Geoscience Center in Göttingen (Isotope Geology Division, Göttingen University).

Gas tank	Used for	c [ppm]	δ^{13}C [‰VPDB]	δ^{18}O [‰VPDB-CO2]
Pure CO_2 'ambient CO_2'	δ-calibration & „referencing"	-	-9.94 ± 0.01	-17.5 ± 0.3
Pure CO_2 'bio CO_2'	δ-calibration	-	-28.25 ± 0.01	-27.2 ± 0.3
Syn. air with CO_2 'SACO2-1'	c-calibration (Low Standard)	349.5 ± 0.1	-37.01 ± 0.02	-34.1 ± 0.4
Syn. air with CO_2 'SACO2-2'	c-calibration (High Standard)	453.9 ± 0.1	-36.98 ± 0.02	-34.2 ± 0.6
Syn. air with CO_2 'SACO2-3'	evaluating c-calibration	349.6 ± 0.1	-37.02 ± 0.01	-34.3 ± 0.4
Syn. air with CO_2 'SACO2-4'	evaluating c-calibration	453.2 ± 0.1	-37.02 ± 0.02	-34.8 ± 0.4
Pressurized air 'PA-tank'	evaluating c-cal. & accuracy test	413.7 ± 0.2	-9.7 ± 0.2	-5.3 ± 0.4
Syn. air with CO_2 'SACO2-5'	long term stability test	396.5 ± 0.1	-37.02 ± 0.02	-34.7 ± 0.2

Table 4. Validation of the multilayer model CANVEG using Eddy Covariance measurements of gross primary productivity GPP, net ecosystem exchange NEE, latent and sensible heat flux LE and H. Slopes, R^2 values and normalized standard error estimates NSEE of linear regressions between modeled and measured values are comparable to the numbers given by (Knohl and Baldocchi, 2008).

	SLOPE	R^2	NSEE
GPP	0.92	0.90	0.26
NEE	0.97	0.92	0.28
LE	1.03	0.78	0.16
H	0.96	0.87	0.37

Table 5. Allan deviation σ_A for different averaging times τ, with the minimum Allan deviation for $\tau_{\min} \approx 290\,s$ for both δ-values and 170 s for CO_2 concentration c

τ [s]	$\delta^{13}C$ [‰]	$\delta^{18}O$ [‰]	c [ppm]
1	0.29	0.40	0.09
20	0.06	0.09	0.02
80	0.03	0.05	0.02
$\tau_{\min}$	0.02	0.03	0.007
500	0.03	0.04	0.01
1800	0.03	0.08	0.01

Table 6. Power consumption of the installation at the field site - measured after all components were thermally stabilized

Power consumption	
δ- Ray analyzer	approximately 220 W
Profile system pump (purges 6 mm OD tubing)	approximately 70 W
Basic infrastructure (contains heated tubing)	approximately 260 W

Table 7. Percentage of total measurement time for major data gaps. The latter two data gaps concerned only target gas measurements.

Reason for data gap	Percentage
Data acquisition problems	6.0 %
Laser alignment problem	5.3 %
Calibration	1.5 %
Power failures	3.3 %
Additional measurements	1.6 %
Plumbing issues (only target)	9.5 %
Switching unit failure (only target)	0.7 %

Table 8. R^2 values for correlations between the ^{18}O composition of ecosystem respiration $R_{eco}^{18}O$ and different meteorological variables. Significance thresholds are given by *** for $p<10^{-4}$; ** for $p<10^{-3}$ and * for $p<10^{-2}$. For some parameters the height above the ground (with negative values indicating the depth below the ground) is given in brackets, the parameters without such indication are measured 42 m above the ground.

	All periods	Before the snow	After the snow
Soil moisture (-8 cm)	0.48 ***	0.00	0.00
Upwards shortwave radiation	0.41 ***	0.28 *	0.15
VPD	0.18 **	0.09	0.25
Soil temperature (-8 to -64 cm)	0.39 ***	0.06	0.70 ***
Air Temperature	0.26 ***	0.02	0.63 ***
Air Temperature (2 m)	0.25 ***	0.05	0.62 ***
Upwards longwave radiation	0.24 ***	0.02	0.62 ***
Incoming longwave radiation	0.04	0.49 ***	0.03
Ambient pressure	0.05	0.39 ***	0.40 *
Incoming shortwave radiation	0.38 ***	0.25 **	0.21
Dewpoint temperature	0.04	0.38 ***	0.19
Specific humidity	0.03	0.35 ***	0.22
H_2O concentration	0.03	0.35 ***	0.22
Actual vapor pressure	0.03	0.34 ***	0.23
Relative humidity	0.29 ***	0.31 ***	0.18
Rain	0.04	0.29 **	0.12

Appendix A: Measures to improve data quality

To reduce the uncertainty of the calculated isotopic composition of ecosystem respiration $R_{\mathrm{eco}}^{13}C$ and $R_{\mathrm{eco}}^{18}O$, we used the following approaches concerning setup and post-processing.

– **Minimizing the sampling time**

5   One of the key assumptions of the Keeling-Plot approach Eq. (1) is the mixing of a constant background with one (integrated) source. This assumption is justified, if there is no significant change in the background concentration c_{bg}, its isotopic composition δ_{bg}, and the isotopic composition of the (integrated) source δ_s for all data points that are taken into account for a single Keeling-Plot. For the case of an integrated source, a constant δ_s can be ensured when the isotopic composition of the individual source components $\delta s, i$ as well as the relative contribution of the individual source components α_i in Eq. (2) are constant. As in general all these quantities

10   ($\delta_{s,i}$, α_i, c_{bg} and δ_{bg}) can vary with time, this assumption tends to be violated stronger for longer measurement times. Thus, the uncertainty of calculated Keeling plot intercepts can be reduced by minimizing the measurement time, as discussed e.g. by Bowling et al. (2003b),who recommend to use only measurements that took less than five hours for analyzing Keeling-Plot intercepts for $\delta^{18}O$. As our setup measures all the nine heights within 30 minutes, we were also able to calculate Keeling-Plots for even shorter periods. During data analysis we calculated Keeling-Plots on timescales between 30 min and 5 h.

15   – **Increasing the CO_2 concentration range**

The linear regression that underlies the Keeling-Plot, can be improved significantly by increasing the CO_2 concentration (Zobitz et al., 2006). In our setup, we increase the CO_2 concentration range by using data from all nine inlet heights within one Keeling-Plot, but this, on the other hand, could violate the assumption of constant relative contributions of the individual source components α_i in Eq. (2) to the integrated source. To analyze if there are any biases due to the inclusion of the different inlet positions, we evaluated

20   the Keeling-Plots for the lower inlets (heights 1-4) and for all all inlets (heights 1-9) separately. The difference Δ between the these differently calculated Keeling-Plot intercepts showed a symmetric frequency distribution around 0 (Fig. S1 in the supplementary material) and by including all heights into the data analysis, we could reduce the error of the intercept σ significantly from a mean value of $\overline{\sigma_{low}} \approx 1.5\permil$ to $\overline{\sigma_{all}} \approx 0.8\permil$ for both isotopic species. These numbers refer to a Keeling-Plot that includes data from three consecutive measurement cycles, yielding a temporal resolution of 90 min. Reasons for the choice of this time resolution are given

25   below.

– **Performing an ordinary Model I regression instead of a Model II regression**

We used an ordinary Model I regression instead of a Model II regression. According to Zobitz et al. (2006), this approach takes into account that the error of the measured δ-values dominates over the error of the measured concentrations and yields unbiased estimates of the Keeling-Plot intercept. In our setup the application of a Model I regression can be justified by the fact that the relative precision

30   of δ measurements is more than an order of magnitude larger than the relative precision of the CO_2 concentration measurements: To estimate the relative uncertainty of the three measured quantities, we calculated the ratio of Allan Deviation at our measurement time of 20 s over the typical range of c, $\delta^{13}C$ and $\delta^{18}O$. The typical range, we further define as the median of the range we obtained in one of our 30 min measurement cycles. Thus, with Allan deviations of 0.02 ppm, 0.06 ‰ and 0.09 ‰ and typical ranges of 26 ppm, 1.5 ‰ and 1.1 ‰ for c, $\delta^{13}C$ and $\delta^{18}O$, we get relative precisions in the order of 10^{-3} for CO_2 10^{-2} for $\delta^{13}C$ to 10^{-1} for $\delta^{18}O$. Thus, the

35   relative precision of the concentration measurement is at least an order of magnitude better than the relative precision of concentration measurements.

– **Filtering data to get only high quality linear regressions**

Data filtering to remove bad quality and biased (Model II) linear regressions has been often done by excluding data with a to low CO_2 concentration range (Pataki et al., 2003; Bowling et al., 2005). Whereas Pataki et al. (2003) recommend to exclude all data from the analysis that spans a CO_2 range below 75 ppm, Bowling et al. (2005) choose this threshold to be 40 ppm. This data filtering approach,

5   based on CO_2 concentration range, does not seem necessary when applying a Model I regression: Zobitz et al. (2006) analyzed consequences of small CO_2 concentration ranges numerical as well as analytical and conclude that for Keeling-Plot intercepts based on Model I regressions 1) a bias at low CO_2 concentration ranges in not expected at current analytical error levels and 2) that errors in the intercept can be small, even for small CO_2 concentration ranges if the δ-values are measured accurately enough. Figure S2 in the supplementary material shows the relationship between CO_2 concentration range and the standard error of the intercept σ for a

10   measurement period of 30 minutes. This figure also shows two comparable approaches for data filtering that both accept 85 % of the data: One approach would be to directly remove data with large intercept errors, and the other approach, as mentioned above, is to remove data with to low CO_2-range. As visible in Fig. S2 in the supplementary material, this approach would remove considerable amounts of data with a very small σ which might be good quality data. For this reason (and as we do not expect a bias occurring for small CO_2 concentration ranges for our Model I type regression), we decide for a direct filtering based on a σ-threshold and used the

15   85 % data points with the smallest standard error σ.

– **Removing outliers**

Our set-up, based on the measurement of $\delta^{13}C$, $\delta^{18}O$ and CO_2 concentration c, enabled us in principal to calculate individual Keeling-Plots based on all inlets (heights 1-9) with a temporal resolution of 30 min. We calculated Keeling-Plots on different timescales ranging from 30 min to 5 h by using one to ten measurement cycles and evaluated how the calculated Keeling-Plot intercepts $\delta^{13}C_{KP}$ and the

20   corresponding standard errors of the linear regression σ changed (Fig. S3 in the supplementary material). As expected, the error of the intercept σ could be reduced by including more measurement cycles. Additionally, the range of calculated Keeling-Plot intercepts reduced considerably: Keeling-Plot intercepts that are based on 30 min timescales included much more data points far beyond the range of Keeling Plot Intercepts on longer timescales. For timescales of 2 h to 5 h there were only few data points with Keeling plot intercepts below -33‰ and above -25‰, which would also be unreasonable numbers: For a timescale of 2 h 3 % of the total

25   calculated data points were out of this range, whereas for timescales of 5 h only 1 % of the data points were outside of this range. As the range of the Keeling-Plot intercepts should not depend on the chosen timescale, we considered the Keeling-Plot intercepts outside of this range as outliers and removed them from the consecutive data analysis.

– **Choosing a time resolution for individual Keeling-Plots**

To decide for a suitable time resolution to analyze the temporal variability of the Keeling-Plot intercepts, we had to solve the threshold

30   between 1) more accurate data on longer timescales and 2) a larger number of data points that were available (after the above mentioned filtering procedures). We decided to fit the individual Keeling Plots on 90 min resolution, which yield a maximal number of $N_{filtered} \approx$ 2350 accepted data points and standard errors σ with a median of 0.76‰ (Fig. S4 in the supplementary material).

– **Calculation of weighted means for nighttime data**

For analyzing variations in the ecosystems respiration R_{eco} on seasonal timescales we used the (filtered) individual Keeling-Plots,

35   each based on 90 minutes of input data, and calculated the mean over all Keeling-Plots that were collected between 9h30 pm and 2h30 am (using the weight w based on with the standard error σ of the Keeling-Plot intercept: $w = 1/\sigma^2$).